Development of Hydrogel-based Porous Desiccants for Atmospheric Water Extraction

by

Xingbang Zhao

A Thesis Presented in Partial Fulfillment
of the Requirements for the Degree
Master of Science

Approved July 2021 by the
Graduate Supervisory Committee:

Lenore Dai, Chair
Paul Westerhoff
Yang Jiao

ARIZONA STATE UNIVERSITY

August 2021

ABSTRACT

Atmospheric water extraction (AWE) is an emerging technology to tackle water resource shortage challenges. One such approach to provide fresh water utilizes stimuli-responsive hydrogel-based desiccants to capture the moisture from the air and release it into the liquid form. Typical gel desiccants are composed of a hygroscopic agent for capturing and a hydrophilic gel matrix for storage. The desorption process can be completed by elevating the temperature above the upper or lower critical solution temperature point to initiate the volume phase transition of either thermo-responsive or photothermal types.

This thesis focuses on investigating the structural effect of hydrogels on moisture uptake. Firstly, the main matrix of gel desiccant, poly(*N*-isopropylacrylamide) hydrogel, was optimized via tuning synthesis temperature and initial monomer concentration. Secondly, a series of hydrogel-based desiccants consisting of a hygroscopic material, vinyl imidazole, and optimized poly(*N*-isopropylacrylamide) gel matrix were synthesized with different network structures. The moisture uptake result showed that the gel desiccant with an interpenetrating polymeric network (IPN) resulted in the best-performing moisture capturing. The gel desiccant with the best performance will be used as a primary structural unit to evaluate the feasibility of developing a light-responsive gel desiccant to materialize light-trigger moisture desorption for AWE technology in the future.

Dedication

To my family for their nurture and edification

ACKNOWLEDGMENTS

First, I would like to sincerely thank my advisor, Prof. Lenore Dai for her approval to join the research group and give me a chance to be involved in this project. I am very grateful for her patience, guidance, encouragement, and thoughtfulness. Her careful educating has always been leading me to advance my master's degree adventure constantly.

Second, I would also like to express my sincere thanks to Prof. Paul Westerhoff and Prof. Yang Jiao for serving as my committee members and all the valuable suggestions and resources they have given to me.

I would take this opportunity to appreciate the lab members from the Dr. Dai's group. Wendy Lin spent much time discussing with me on all lab stuff, urging and cultivating me to study and think more; Dr. Ryan Gunckel gave me many insightful advice on sample synthesis, materials choice, and apparatus usage; Dr. Yifei Xu supervised me in the early days when I joined the group, trained me in hydrogel synthesis; Dr. Marisa Gliege, Chris Whitney, and Mu-Tao Chen, helped me with equipment operation and presentation that accelerates the experiments and boosts my confidence. I would also like to thank Prof. Westerhoff's lab members, Dr. Chao Zeng and Prof. Anjali Mulchandani for their equipment training and valuable discussion.

Last but not least, I would like to thank all my family members for their love that nourish and accompany me on my way to chase my dream. Thanks to my friends whom I met in Arizona. We are all in it together, getting through the hard times of the pandemic.

TABLE OF CONTENTS

Page

CHAPTER Page

LIST OF TABLES

Table Page

Table Page

LIST OF FIGURES

Figure Page

Figure Page

Figure Page

Figure Page

CHAPTER 1

INTRODUCTION

1.1 Atmospheric Water Extraction Technology

Deepening shortage of water resources on Earth, yet the demand for clean drinking water continuously keeps rising because of rapid population growth and industrial technology. Globally, two billion people live in countries and areas with water stress, and half the population will live in the water-stressed areas by 2025 [1,2]. More severely, water-borne diseases from contaminated water such as diarrhea, cholera, and dysentery will have a detrimental effect on human health [2]. Therefore, looking for viable resources to supply clean water is a global necessity. Recent studies showed that atmospheric water is an abundant reservoir of freshwater that acts as a neat resource for those water-deficient areas for drinking and agricultural purposes [3,4]. Moreover, it conserves the substantial exploitable waters, equivalent to roughly 10% of the water in all lakes on Earth [5,6]. Therefore, atmospheric water extraction (AWE) technology could be developed to harvest atmospheric water for daily use [7].

Generally, there are three types of atmospheric water — clouds, fog, and water vapor in the air (moisture) — considered as a water resource [8]. Clouds and fog are all inundated with tiny water droplets. However, these modes require the high-RH (relative humidity; usually 100%) environment conditions, which is different from the low-RH

places [9,10]. The design criteria of the third collection mode must include strategies to capture the moisture from the air and efficiently release it in liquid form. A typical method is so-called dew water capturing, which utilizes the water vapor condensation process when the temperature goes below the dew point temperature of water molecules to form water droplets [11]. Certain commercial hygroscopic materials, such as deliquescent salts and silica gel, could materialize the process due to their affinity with water through the adsorption and absorption phenomena [6,12,13]. Once the moisture capturing process is finished, moisture desorption could be realized via heating to increase the vapor pressure at the surface of hygroscopic materials.

Deliquescent salts exhibit stronger affinity among the hygroscopic materials; however, performing substantial water extraction from salts is challenging. The hydration of hygroscopic salts will produce an aqueous solution or clumpy salts. More seriously, although each material functions well at specific relative humidity, none can operate across a wide range of humidity. Subsequently, a type of composite gel desiccant made by incorporating hygroscopic materials into a thermo-responsive hydrogel matrix is suggested to handle the atmospheric water extraction technology [14,15]. These two studies represented a skillful design for moisture capturing, storage, and release, transporting adsorbed water molecules from hygroscopic materials into the hydrophilic matrix for storage [14,15]. Applying an external stimulus, higher temperature, on the composite to induce the volume phase transition (hydrophilic/hydrophobic) enables the water desorption [14,15]. However, even a hydrogel-based desiccant has potential

drawbacks from long-term usage if salts are applied as hygroscopic agents. Deliquescent salts in the gel desiccant system may be subjected to salts leakage due to the lower compatibility.

Current design motifs expect hydrogel-based desiccants with superior characteristics like faster sorption-desorption kinetics and multiple stable cycles of performance through rational structural design. These outstanding features would surely allow hydrogel-based desiccants to become more of a magnet for atmospheric water extraction technology.

To the best of our knowledge, only a finite publication briefly described the structure of hydrogel-based desiccants. Moreover, no one has systematically investigated structural effects on the moisture uptake performance of gel desiccants. Hence, it is of good interest to better understand how different compositions and structures affect the moisture uptake performance of hydrogel-based desiccants. Furthermore, the goal is to determine the efficient structural unit that could also be utilized further to develop hydrogel-based desiccant for future valuable AWE technology applications.

1.2 Structure of Thesis

Chapter 1 introduces a brief background of AWE technology and current approaches for this technology. Besides, it describes the motivation of the thesis on the study of structural effects on the moisture uptake performance of hydrogel-based desiccant.

Chapter 2 presents a detailed introduction about stimuli-responsive hydrogels, hygroscopic materials, and gel desiccants for AWE technology. It also explains the motivation for thesis work in detail.

Chapter 3 describes the experimental methodology, including synthesizing poly(*N*-isopropylacrylamide) (poly-NIPAm) hydrogels and synthesizing gel desiccants. Moreover, a quick overview of characterization methods like liquid water uptake tests, water retention tests, moisture uptake tests, and heat analysis is described.

Chapter 4 discusses the investigation process of approaching the best structural unit for developing hydrogel-based desiccant for AWE technology. Firstly, the optimized poly-NIPAm hydrogel was selected through the liquid water uptake and water retention tests. Secondly, the gel desiccant with the more suitable network structure was selected through the moisture uptake tests.

Chapter 5 summarizes the thesis work on the development of porous hydrogel-based desiccant for AWE technology. Furthermore, the future direction is described and proposed, exploring the feasibility of using a novel stimulus as a trigger to initiate the moisture desorption process.

CHAPTER 2

BACKGROUND AND MOTIVATION

2.1 Stimuli-Responsive Hydrogels

Hydrogels are a species of cross-linked polymer that is highly hydrophilic. These gels can swell and contract, all while retaining a remarkable portion of water within their three-dimensional networks. The three-dimensional networks can be linked via physical or chemical linkage junctions, for example, ionic interactions, hydrogen bonds, and polymer chain entanglement. All these routes will enable hydrogels to have specific swelling capabilities. Furthermore, its equilibrium swelling ratio can be ameliorated by introducing more hydrophilic functional groups on the backbone of the monomer of a hydrogel, such as an amide, carboxyl, and hydroxyl [16]. In addition to this prominent water retention ability, introducing any other functional compounds into the monomer's backbone will revolutionize the properties of hydrogels to a fascinating level. Fabricating hydrogel-based composites has been given whole new meanings. Therefore, hydrogels can be divided into various subgroups based on their different property, as summarized in Figure 2.1.

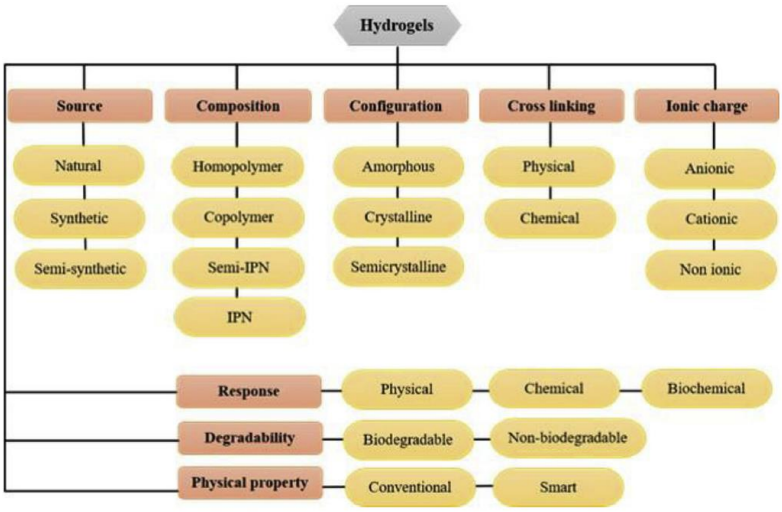

Figure 2.1. Classification of hydrogels (adapted from [17])

Stimuli-responsive hydrogels are one subtype of hydrogels that intelligently respond to external stimuli like mechanical [18], pH [19], glucose [20], temperature [21-23], visible light [24-26], electric field [27], and magnetic field effects [28]. In view of this, such a subclass of functional hydrogel materials can be further categorized based on the type of external stimulus. Generally, hydrogels' intelligent response would include a reversible phase transition, such as a change of shape, morphology, surface characteristics, and solubility. Stimuli-responsive hydrogels are particularly concerning due to their extensive application prospects. By virtue of these 'smart' response behaviors, many researchers have brought a mass of smart and functional devices to the public in the past few years that applying stimuli-responsive hydrogels to an actuator [29], glucose sensor [30], mechanical sensor [31], and controlled drug delivery system [32-34], along with flexible electronics such as artificial skins [35], and even treatments for diabetic ulcers and gastric devices [36,37].

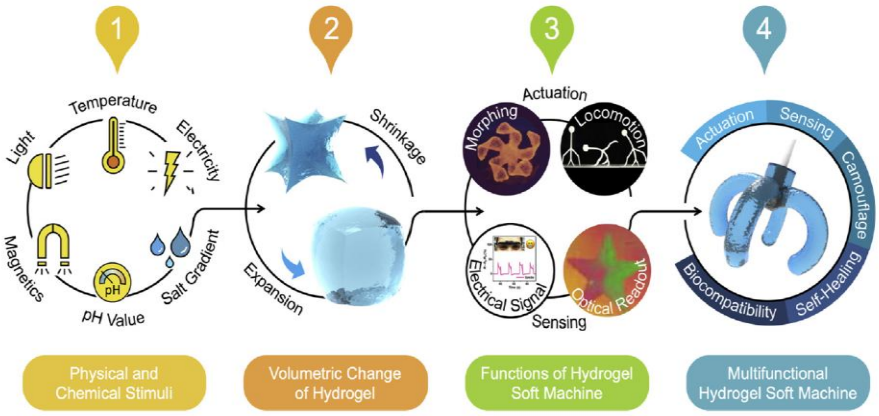

Figure 2.2. Different types of stimuli-responsive hydrogels, volume transition, and enabled applications (adapted from [38-42].

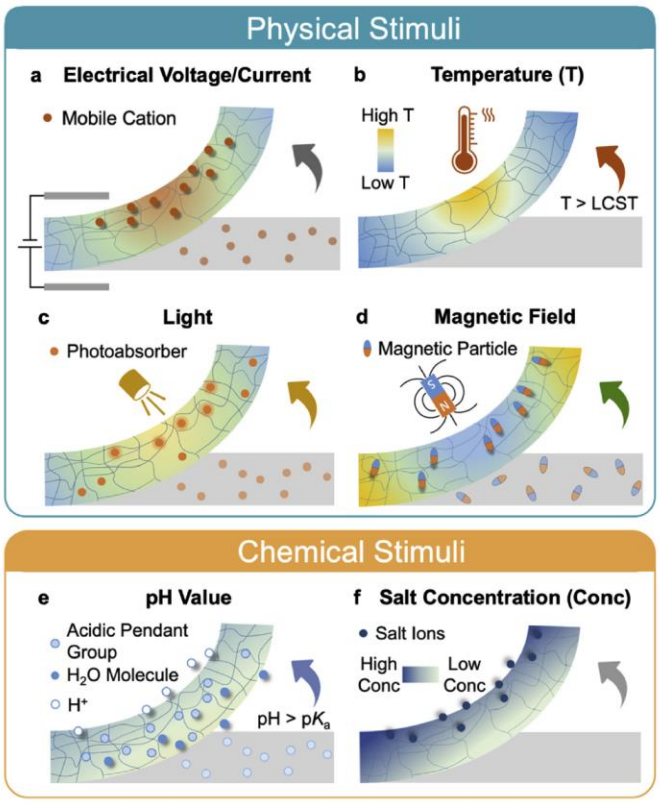

Figure 2.3. Mechanism of different types of stimuli-responsive hydrogels (adapted from [38]).

Thermo-responsive Hydrogels

Thermo-responsive hydrogels are well-studied functional gel materials. Such materials are classified into two main types on the basis of the critical temperature that they start to show the volume phase transition. First, hydrogels that swell below the critical temperature and shrink above the critical temperature upon heating are lower critical solution temperature (LCST) types. Second, the upper critical solution temperature (UCST) type possesses the opposite behavior compared to the LCST type.

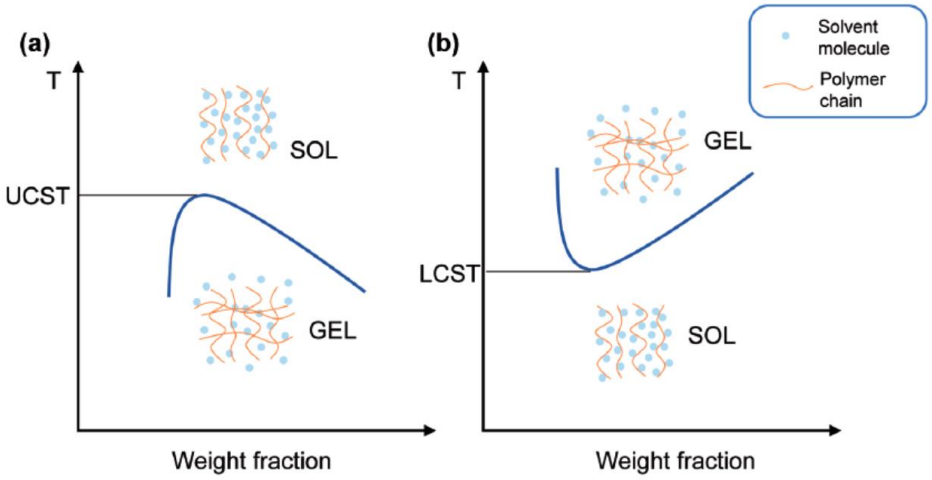

Figure 2.4. Thermo-responsive hydrogels: (a) UCST type that undergo phase transition when temperature decreases and (b) LCST type that undergo phase transition when temperature rises (adapted from [43]).

Thermo-responsive hydrogels usually have different characteristic functional groups on their backbone. For example, poly (*N*-isopropyl acrylamide) (Poly-NIPAm), a typical LCST type hydrogel, has hydrophilic amide and hydrophobic isopropyl groups in Figure 2.5 shows. The interaction effect between either hydrophilic or hydrophobic functional groups with solvent plays a role in the volume phase change that Flory-Higgins theory theoretically supports. It thoroughly elaborated the relationship between three different

interactions among polymers and solvents and the shrinkage of the LCST type hydrogel. It appears due to the diminution of polymer-solvent interaction when the temperature is above a specific point. The decreased polymer-solvent interaction would bring more polymer-polymer interactions so that the hydrophobic effect would dominate. However, the Flory-Higgins theory builds upon an ideal mixture condition, which may ignore the actual situation of anisotropic interaction such as dipole-dipole interactions, H-bonds, and electrostatic effect when a polymer contacts the solvents. Considering the volume transition behaviors from the Gibbs free energy equation perspective, when the temperature is below the critical temperature point, the hydrogen bond would form between hydrophilic amide groups and water molecules. The water molecules would then be well-organized to obtain a negative value to entropy (ΔS). When the temperature exceeds the critical temperature point, the entropy (ΔS) of the system will increase, resulting in the breakage of the hydrogen bonds. An increment of hydrophobic interactions from the breaking of hydrogen bonds usually generates chain collapse and intermolecular aggregation. Therefore, a negative value to Gibbs free energy (ΔG) from the equation $\Delta G = \Delta H - T\Delta S$ initiates the volume phase transition.

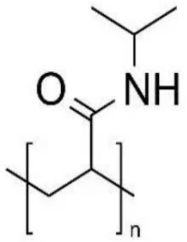

Figure 2.5. Chemical structure of Poly-NIPAm

Contrasting LCST type hydrogels, UCST type hydrogel materials are rarely published regarding the fabrication of smart devices. A representative UCST type hydrogel is fabricated in the interpenetrating polymeric network (IPN) made up of interlocking phases of acrylamide (AAm) and acrylic acid (AAc) [44]. This work displayed that hydrogen bonds between the acrylamide and acrylic acid networks would drive the gel to fall in at low temperatures. When temperature increases, the enthalpy of these hydrogen bonds would enlarge to disrupt due to the entropy loss of the water molecules, thereby hydrating the polymer network. Therefore, such an IPN hydrogel showed a higher swelling ratio at higher temperature conditions. In short, the volume phase transition process of LCST type hydrogels is entropically driven while UCST type hydrogels' process is enthalpically driven.

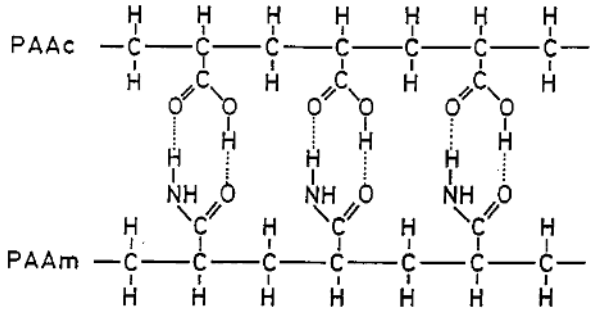

Figure 2.6. The formation of hydrogen bonds between poly-acrylic acid and poly-acrylamide (adapted from [44]).

The intelligent reversible hydrophilic/hydrophobic behavior is a magnet for many applications. Poly-NIPAm and poly (*N*-vinylcaprolactam) (Poly-NVCL) have been widely utilized because they present phase changes close to the physiological temperature of the human body. With an eye to the more biocompatible nature of Poly-NVCL [45],

Sudhakar et al [46] studied the feasibility of Poly-NVCL as a leading controlled drug-release system for targeted therapy. The previous studies showed that the poor solubility and oral bioavailability of the drug, curcumin, are major developmental obstacles [47]. Taking these factors into account, the author fabricated a curcumin-encapsulated cross-linked poly (NVCL-co-HEMA) hydrogel in two steps. Firstly, the poly (NVCL-co-HEMA) is polymerized through free radical emulsion polymerization. Then the curcumin is loaded into the copolymer gel using the *in situ* method. Such a hydrogel still shows temperature sensitivity due to the presence of Poly-NVCL. Below LCST, the release rate of curcumin from copolymer hydrogel is fast, whereas, above LCST, the drug release decreases due to hydrogel's abrupt hydration effect, change from hydrophilic to hydrophobic. An intelligent delivery system based on biocompatible thermo-responsive hydrogel helps improve targeted drug delivery applications' feasibility and efficiency.

Light-responsive Hydrogels

In recent years, scientific researchers have started investigating light-responsive hydrogels. Light, a forthright stimulus, can instantaneously trigger a more accurate and precise phase transition without requiring high energy compared to other stimuli. Light-responsive hydrogels extend more possibilities stimuli-trigger hydrogel-based functional devices applied to the biomedical, energy, and environmental fields. All light-responsive hydrogel-based functional devices can be divided into two main categories in the light of the first criterion, mechanism of responsive behaviors.

First, previous works described why hydrogels possess light-responsive behaviors due to the photothermal effect. This approach to developing light-responsive hydrogels builds a solar photothermal agent in the gel system. The agent should convert the absorbed incident light energy to heat energy, thereby heating the local samples and initiating the phase transition. The representative photothermal agents used in photothermal hydrogels are carbon nanotubes [48,49] and graphene oxide [50] since they have outstanding properties such as high light absorbance and conversion efficiency. Moreover, the photothermal agent embedded in the gel system directly renders light-responsive hydrogels' responsive wavelength because photothermal agents show different optical absorption. This criterion is precisely the second distinguishing feature that further differentiates photo-responsive hydrogels on the grounds of a light source wavelength to which they could respond. Although photothermal genre hydrogels have been utilized as cleanup devices for heavy oil spills [49] and near-infrared therapy drug delivery systems [51], they have not been widely researched due to the high energy requirements.

The second mechanism of light-responsive behaviors is usually called direct light-responsive due to the presence of photosensitive moieties in the gel systems. Specifically, azobenzene and spiropyran are photosensitive moieties that have been studied at length [52-54]. When integrating photosensitive moieties into the gel systems, the hydrogel will display a reversible sol-gel transition via photoisomerization. These moieties would be reversibly transformed *cis* to *trans* after stimulation by a specific light wavelength [55].

Therefore, such intelligent responsive behaviors materialized the possibilities for the sensing application in drug delivery devices [56] and actuators [57,58]. Researchers from Northwestern University recently developed a bi-layered spiropyran-based hydrogel actuator that can freely crawl like an inchworm or octopus via the switch on and off the light source [59]. More interestingly, through the synergistic photo-actuation effect of the layer's swelling and deswelling behaviors and predetermined coding procedure, the hydrogel actuator can also possess the origami-like shape transformation under light irradiation.

As mentioned above, light-responsive hydrogel materials hold promise in various fields but still suffer from fundamental limitations. These limitations nudge researchers to design strategies to speed up their responsive kinetics and improve sensitivity, which will not risk hydrogel's mechanical properties for cycle operation. In addition, such design strategies also work for other types of stimuli-responsive hydrogel materials.

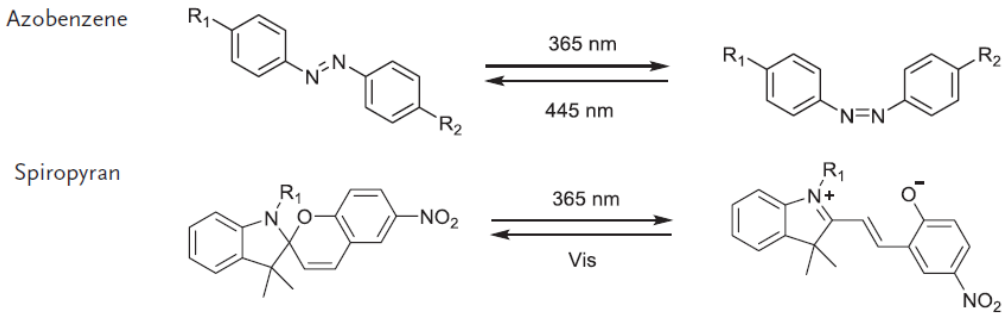

Figure 2.7. The isomerization of photosensitive moieties (adapted from [52]).

2.2 Hygroscopic Materials

Hygroscopic materials represent a group of materials that capture moisture from the air. The first group of hygroscopic materials is in liquid forms, such as glycol-contained organic liquid desiccants, used as glycol dehydration agents for industrial machinery. Other examples include a cluster of deliquescent salts, like calcium chloride, lithium chloride, and copper (II) nitrate. Li and his colleagues screened the hygroscopicity of fourteen different anhydrous deliquescent salts for AWE technology with sunlight as the sole energy source [60]. They found that copper chloride is more suitable for use in desert regions where is low ambient RH and abundant sunlight irradiation. Meanwhile, $CuSO_4$ and $MgSO_4$ are preferable for high humidity regions with low sunlight irradiation, such as island or mountain areas [60].

A significant limitation of using deliquescent salts is forming a salt solution after capturing saturated water vapor. For example, calcium chloride, a general deliquescent salt used daily, may transform into lumps and become a saturated salt solution if it comes in complete contact with the air. Such a process is called deliquescence, which is driven by the pressure difference between partial pressure of water vapor in the environment and vapor pressure of salts surface. Under such circumstances, deliquescence continuously happens until dissolving itself into an aqueous solution. The following water desorption would be a complicated task since salt solution formed so that a high temperature is required.

Solid hygroscopic materials are generally described as solid desiccants or adsorbents. The capturing mechanism of such a subgroup of materials usually adsorbs moisture from the air onto their surface by physisorption due to the weak van der Waals force. Commonly used solid hygroscopic materials, silica gel, adsorbs water through the interaction between the hydroxyl group on the silica gel surface and moisture in the air. Once it reaches the equilibrium state, the caught moisture could be oozed via high-temperature heating. Another example, MOFs, are a class of three-dimensional hybrid material consisting of metal ions linked by organic ligands. MOFs take advantage of structural properties to capture moisture via chemisorption, where moisture would be adsorbed onto the metallic clusters [61-63]. The water release process of saturated solid hygroscopic materials may require either exposure to the solar irradiation or incorporation with a condenser that would utilize condensation by direct cooling below the dew point [13,63].

2.3 Gel Desiccants for AWE Technology

The aforementioned hygroscopic materials are all typical options that can be supplied for atmospheric water extraction technology. However, extensive heat energy consumption is a vital factor that nudges researchers looking for an alternative. Liu et al proffered a new concept, ‘hydrogel machine’; described the potential of functional hydrogel materials in actuators, coatings, and even atmospheric water harvester areas [7]. It reviewed and clarified hydrogel-based atmospheric water harvester machines based on the approaches to initiate water release.

One of them is a photothermal agent such as carbon nanotube or pyrrole to convert the two types of energy to make the release process faster [64,65]. In addition to the photothermal agent, another work directly uses thermo-responsive composite gel material as the principal platform for atmospheric water extraction [14]. The strategy used in these systems covers the moisture capture by deliquescent salts and transportation of absorbed water vapor from the gel surface to the hydrophilic gel matrix. A three-dimensional hydrogel network can hold the absorbed water vapor where it acts as a platform to keep the water and impede the deliquescent salt from becoming the salt solution. For the water release process, a temperature above the LCST of thermo-responsive hydrogel would induce the volume phase transition to retrieve the liquid water at the end.

On top of that, deliquescent salt has also been shown to integrate with MOFs as composite sorbents. They capitalize on both the porous supporting matrix and deliquescent salts [66]. After embedding salts, composite sorbents for AWE technology

own the faster capturing kinetic and preferable cycling stability than single hygroscopic desiccants. However, the limitation may remain that hygroscopic salts are leaking out of the storage matrix during the desorption process due to poor compatibility. Consequently, hygroscopic polymers were exploited as moisture capturing agents instead of salts to validate more possibilities for AWE technology research. Zhao and colleagues created a super moisture absorbent gel using polypyrrole-chloride and poly-NIPAm [15]. Having the large net surface areas in contact with moisture enables polypyrrole-chloride to show superexcellent moisture uptake capacity. Thermo-responsive poly-NIPAm acts as the 'smart' component in the gel desiccant system to respond to the heat stimulus, initiating the water release.

2.4 Motivation of Work

2.4.1 Water Uptake Capacity Optimization of Poly (*N*-Isopropylacrylamide) Hydrogel

The papers described above have shown many designing schemes for AWE technology. In general, a hydrophilic hydrogel matrix coupling with a hygroscopic material is the fundamental unit for desiccants. Furthermore, a photothermal agent might be incorporated into the gel desiccant system depending on the type of triggers for moisture desorption. However, they may be considered energy-intensive on the grounds of power consumption because they rely upon heat to desorb adsorbed water molecules. A lower energy demand gel desiccant with faster sorption-desorption kinetics would satisfy the advancement needs.

Supporting platform, the hydrophilic hydrogel matrix plays a vital role in the gel desiccant system because it stores the adsorbed moisture from the air within its matrix. Consequently, its swelling performance is one of the determining factors that influence the moisture uptake capacity of the gel desiccant. The more the swelling ratio hydrogel, the larger the liquid water uptake capacity hydrogel may present, which possesses in-depth potential to capture more moisture. Therefore, reasonable regulation of the internal structure form could steadily optimize the property of hydrogel-based desiccant to meet particular expectations.

This work was firstly about optimizing the liquid water uptake capacity of the gel matrix. Undoubtedly, such an essential attribute would be a critical step for developing gel desiccant for AWE technology. Ganji et al. [67] summarized the different types of

porous hydrogel in their review paper. Macroporous hydrogels with pore sizes between 0.1 and 1 μm showed faster swelling kinetics than those microporous hydrogels with 0.01 to 0.1 μm pores. Specifically, the synthesis temperature for the poly-NIPAm hydrogel as a crucial variable is adopted to fabricate different porous structures [68]. Therefore, the first approach for this motivation of works was to tune the synthesis temperature. Such an approach prepared different hydrogels to investigate the effect of porous structure on liquid water uptake capacity. Both Poly-NIPAm hydrogels were conducted via swelling test to verify the effect of porous structure on liquid water uptake capacity.

In addition to the effect of porous structure, another hydrogel synthesis parameter that plays a decisive role in swelling ability and kinetics, the chemical composition in the hydrogel system, has also been previously experimented with in the ref [69]. Therefore, the second approach explored the effect of initial monomer concentration on liquid water uptake capacity. Specifically, the number of crosslinkers was fixed at a constant weight, while the amount of monomer was tuned twice. All studies provided significant features that help to figure out the efficient composition with the best liquid water uptake performance for further incorporation with hygroscopic materials.

2.4.2 Integration of Optimized Poly (*N*-Isopropylacrylamide) Hydrogel with Hygroscopic Materials

After understanding the poly-NIPAm-based hydrogel matrix and determining the best composition, the optimized poly-NIPAm hydrogel was incorporated with hygroscopic materials for further detailed studies. The gel desiccant system needs must be designed as an efficient type to avoid the most likely pitfalls. Therefore, poly (N-vinyl imidazole) (Poly-VIM), a hygroscopic polymer, was used as the moisture capturing agent in the designed system. Poly-VIM has been explored in both its gel and copolymeric form for potential application areas such as gene delivery [70], wine production [71], antimicrobial activity [72], and water treatment [73]. Krishnan et al [74] investigated the ion transport kinetics of such synthetic polymers and demonstrated its relative humidity-dependent ionic conductivity phenomena. They deduced poly-VIM's hygroscopic performance through the chemical bond. Figure 2.9 displays the structure of this synthetic polymer. The imidazole pendant groups from poly-VIM provide a lone pair of nitrogen electrons with a higher affinity with hydrogen bonds. As there is no self-donation source from the poly-VIM, the lone pair of nitrogen electrons and hydrogel bonding could capture the water molecules from the outside with fewer challenges [74].

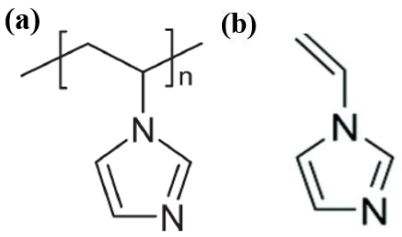

Figure 2.8. Chemical structures: **(a)** Poly-VIM and **(b)** VIM monomer

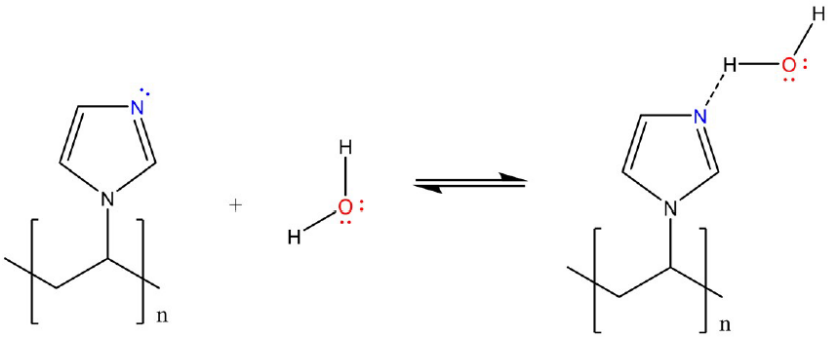

Figure 2.9. The hydration of Poly-VIM via hydrogen bond (adapted from [74]).

To the best of our knowledge, there are no reported works applying vinyl imidazole as one of the main components in hydrogel-based desiccants for AWE technology. In other words, this work is firstly to study the hygroscopicity of vinyl imidazole for AWE technology. Vinyl imidazole-contained gel desiccants were synthesized using the low temperature synthesis method. Notably, these gel desiccants with different network structures were prepared to investigate the influence of network structure on moisture uptake. Hydrogels can be classified into homopolymeric, copolymeric, and multi polymer hydrogels (interpenetrating polymeric network structure hydrogel) based on the preparation method [75].

Furthermore, the types of interpenetrating polymeric network (IPN) hydrogels could be separated into full IPN and semi-IPN. When polymers are all crosslinked in the system, either one-pot or sequential ways, the full IPN has high mechanical properties [76,77]. Semi-IPNs are usually prepared by embedding an uncrosslinked linear polymer into the other crosslinked polymer chains, which also presents better mechanical properties than conventional homopolymeric hydrogel [78]. Therefore, the second motivation of work was to investigate the impact of network structure on moisture uptake performance of the gel desiccants. The base unit in the gel desiccant system, poly-NIPAm hydrogel, and a pure poly-VIM hydrogel were used as control samples for the comparison to study how a hygroscopic material exerts its influence on moisture uptake in the gel desiccant system.

CHAPTER 3

EXPERIMENTAL METHODS

3.1 Materials

N-isopropylacrylamide (NIPAm), 1-vinylimidazole, Ammonium persulfate (APS), azobisisobutyronitrile (AIBN) and N, N-Dimethylformamide (DMF)were purchased from Sigma-Aldrich and used without further purification. N, N′ methylenebisacrylamide (MBAA) was purchased from MP Biomedicals and used as received. N, N, N′, N′-tetramethylethylenediamine (TEMED) was purchased from Thermo Scientific and used as supplied.

3.2 Synthesis and Sample Preparation

3.2.1 Synthesis of Porous Poly(*N*-Isopropylacrylamide) Hydrogels

Room Temperature Synthesis Method

The poly-NIPAm hydrogel was started by mixing 660.595 mg NIPAm and 30 mg MBAA in 5 mL pure water, which is purified by Thermo Barnstead Genpure x CAD Water Purification System. Subsequently, 30 μL TEMED as the accelerator was added into monomer solution. Next, this monomer solution was purged under nitrogen for 10 minutes to remove any oxygen which would impede the reaction of free radical polymerization. After a purge, 1 mL initiator solution of APS (228 mg/mL) was added into the monomer solution. The polymerization was reacted at room temperature for 24 hours. The purification of microporous Poly-NIPAm hydrogel was accomplished by immersing it in pure water for a day to remove any unreacted short chains or monomers.

Low Temperature Synthesis Method

The poly-NIPAm hydrogel was synthesized via preparing monomer solution in the presence of 660.595 mg NIPAm, 30 mg MBAA and 5 mL pure water. Subsequently, 30 μL TEMED as the accelerator was added into the monomer solution. The monomer solution was followed by 10 minutes nitrogen purge in a cold-water bath environment at 5℃. The 1 mL initiator solution (228 mg/mL) of APS was then added into the monomer solution at 5℃ to initiate the polymerization reaction. After waiting 2-3 minutes, the polymeric solution was placed into the fridge at around -20 ℃ for 24 hours. The frozen hydrogel was subsequently thawed and immersed in pure water to remove any unreacted monomers for further characterization.

3.2.2 Synthesis of Porous Poly(*N*-Isopropylacrylamide) Hydrogels with Various Monomer Concentration

30 mg MBAA was fixed and mixed with 30 μL TEMED with various amounts of NIPAm in 5 ml of pure water to obtain different trials. The conditions of hydrogel synthesis, the molar ratio of MBAA/NIPAm, and monomer concentration are summarized in Table 3.1. Each trial was purged under nitrogen and added by 1 mL APS (228 mg/mL) solutions at 5◦C. Subsequently, the polymerization solutions were placed into the fridge for 24 hours to finish the polymerization reaction. The frozen hydrogels were finally thawed and immersed in pure water for purification.

Poly-NIPAm Hydrogels	Molar ratio of crosslinker to monomer	Monomer Concentration (g/ml)
Sample 1	1：30	0.132
Sample 2	1：20	0.0840
Sample 3	1：10	0.0442

Table 3.1. Preparation conditions of macroporous poly-NIPAm hydrogels

3.2.3 Synthesis of Gel Desiccants

Copolymeric gel desiccant: Poly (VIM-*co*-NIPAm) gel desiccant was prepared by mixing two monomers, 449.5 mg NIPAm and 150 μL vinyl imidazole in 5 ml of pure water. The monomer solution was added by 60 mg MBAA and 60 μL TEMED. The monomer solution was purged with nitrogen for 10 minutes and followed by adding 1 mL APS solution (228 mg/mL) at 5◦C to initiate the polymerization process. Then, the vial was placed into the fridge for 24 hours to finish the polymerization reaction. Finally, the frozen hydrogel was thawed and purified to remove any short chain of gels for further characterization.

IPN gel desiccant: In a typical synthesis, the poly-VIM powder was firstly prepared following the references [79]. In short, 3 mL VIM, 0.03 g AIBN, and 7 mL DMF were mixed under stirring to have the homogeneous solution. 10 min nitrogen purge was carried, placing the solution at 75 °C with consecutive stirring for 12 h to finish the polymerization. Then, poly-VIM was precipitated, filtered and washed using ethyl acetate. The poly-VIM powder was obtained in pale yellow after fully oven-drying in vacuum at 60 °C.

Next, 1 mL poly-VIM dispersion (0.16 g/mL) was mixed with 446.4 mg NIPAm, 60 mg MBAA and 60 μL TEMED in 10 mL pure water, where poly-VIM dispersion acts as the linear polymer part and NIPAm roles as the crosslinked polymer part in the semi interpenetrating polymeric network system. After purging with nitrogen at 5◦C for 10 minutes, the solution was added the 2 ml APS solution (228 mg/mL) to be initiated the polymerization. Subsequently, the vial was placed in the fridge for 24 hours to let the polymerization finished. At last, thawing and purifying were implemented to remove unreacted monomers for further characterization.

Pure Poly-VIM gel desiccant (Control sample 1): First, 155 μL vinyl imidazole, 60 mg MBAA and 60 μL TEMED were mixed in 5 ml pure water as the monomer solution. The monomer solution was then purged with nitrogen and added by 1 ml APS solution (228 mg/mL) at 5◦C to kick off the polymerization reaction. Next, the polymer solution was placed in the fridge for 24 hours. Finally, the hydrogel was retrieved for thawing and purifying for further comparative studies.

Pure Poly-NIPAm gel desiccant (Control sample 2): The pure poly-NIPAm gel desiccant was prepared by following the method of developing low temperature synthesis poly-NIPAm hydrogel sample 3.

3.3 Materials Characterization

Liquid Water Uptake Tests

The liquid water uptake tests were conducted at room temperature environment via immersing hydrogel samples in water. All hydrogel samples were freeze-dried in vacuum by Free-Zone[1] dryer, Labconco before incubating into the pure water. The liquid water uptake capacities of hydrogels were determined gravimetrically based on their swelling ratio using the following equation.

$$Liquid\ water\ uptake\ capacity = \frac{W_t - W_d}{W_d},$$

Where W_d is the initial weight of dried hydrogel and W_t is the weight of swelled hydrogel at the predetermined time. They are obtained after taking out from water by a plastic tweezer and shaking off twice to remove the excess water on the surface.

Water Retention Tests

The deswelling behaviors of hydrogel sample were studied gravimetrically by monitoring the weight change of hydrogel in a 40 ℃ water bath. Water retention, *WR* is calculated using the following equation.

$$WR = \frac{W_t - W_d}{W_e - W_d} \times 100\%,$$

Where W_t is the weight of swelled hydrogel at predetermined time after taking out from 40 ℃ water by a plastic tweezer and shaking off twice to remove excessive water on the surface, W_e is the weight of equilibrated hydrogel at room temperature and W_d is the initial weight of dried hydrogel. Prior to the water retention tests, each hydrogel sample was incubated in room temperature water for 5 days to reach the equilibrium state.

Moisture Uptake Tests

The moisture uptake tests were setup in a humidity hood formed from an air clean system chamber, an electric fan, a humidifier coupled with a tube, a humidity meter, and a balance. The moisture uptake test results are analyzed and normalized by mass and surface area approaches. Prior to moisture uptake tests, each gel desiccants' sample was cut into small pieces with the same diameter and thickness and followed by freeze drying process. The moisture uptake capacities of each gel desiccants were calculated using the following equations.

$$Moisture\ uptake\ \left(\frac{g}{g}\right) = \frac{m_t - m_d}{m_d}$$

Where m_d is freeze-dried mass, m_t is mass of the sample at given time,

$$Moisture\ uptake\ \left(\frac{g}{cm^2}\right) = \frac{m_t - m_d}{A}$$

Where *A* is net area of sample in contact with moisture in humidity hood.

$$Moisture\ uptake\ \left(\frac{g}{cm^3}\right) = \frac{m_t - m_d}{V}$$

Where *V* is volume of sample in humidity hood.

Differential Scanning Calorimetry

Glass transition temperature (Tg) was estimated via differential scanning calorimeter (DSC), TA Instruments Q20. Before the DSC characterization, all gel specimens were first air-dried at room temperature in a fume hood and followed by vacuum dried to eliminate retained water in their network entirely. A standard heat/cool/heat mode was adopted with the ramp rate of 5 °C min-1, the gas was set in nitrogen with 50.0 ml/min.

Optical microscopy

The morphology observations of porous hydrogels and vinyl imidazole-contained gel desiccants with different network structures were completed using an optical microscope (7X-90X Trinocular Stereo Boom Zoom Microscope, AmScope). Prior to characterization, all hydrogel specimens were freeze-dried by a FreeZone[1] dryer.

3.4 Supplemental Figure

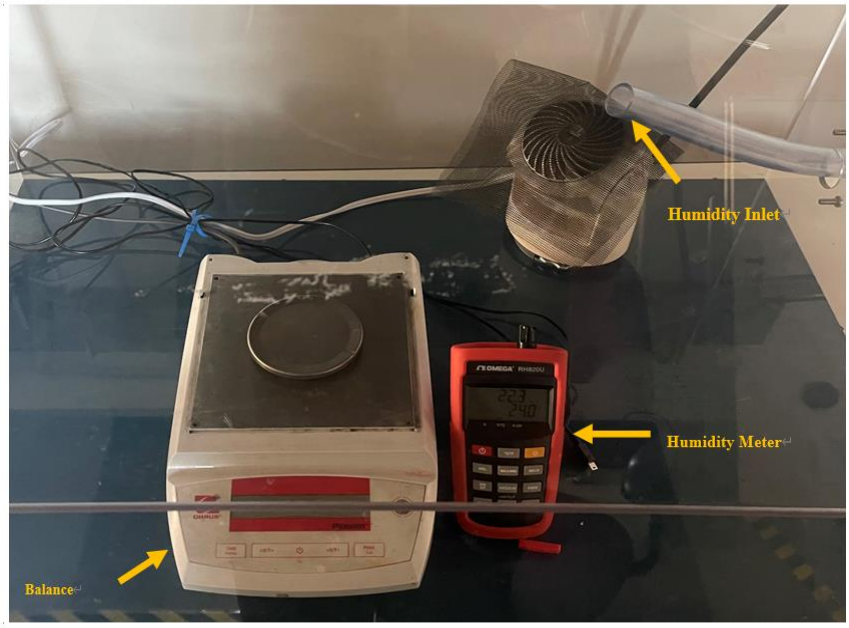

Figure 3.1. The moisture uptake tests setup.

Air clean system chamber contains one balance with data loggers to record the weight change, a humidity sensor to monitor the value of RH%, an electric fan to circulate the humid air, and a humidifier coupled with the tube inlet of humid air. Gel desiccant samples were placed on a glass petri dish and balanced for moisture uptake tests.

CHAPTER 4

RESULTS AND DISCUSSION

4.1 Water Uptake and Release Capacity Optimization of Poly(*N*-Isopropylacrylamide) Hydrogel

4.1.1 Effect of Synthesis Temperature and Porous Structure

The poly-NIPAM hydrogels were synthesized using NIPAm monomers and MBAA crosslinkers, as Figure 4.1 depicts. The crosslinkers tangle the monomer so that the soluble monomer solution is transformed into the bulk gel. Figure 4.2 (a) and Figure 4.3 (a) exhibit two synthesized poly-NIPAm hydrogels that were synthesized differently and photographed via a digital camera. From the visual analysis, in comparison, the room temperature synthesized gels appeared to be a milky white, whereas the low temperature synthesized gel had a more transparent appearance. The poly-NIPAm sample synthesized at room temperature is one of the conventional hydrogels that results in a denser microstructure. In contrast, the low temperature polymerization synthesis is a different method called cryogelation, generating a looser inner structure [80]. The cryogelation, as the name depicts, first occurs under semi-frozen conditions so that the crosslinked network forms around the ice crystal. The subsequent thawing strips away the ice manifold, leaving an interconnected, highly porous network to the cryogel. Therefore, the monomers tangled in the low temperature synthesized hydrogel network are not as close and dense as those in the conventional hydrogel that results from the room temperature synthesis method, leading to a more transparent morphology.

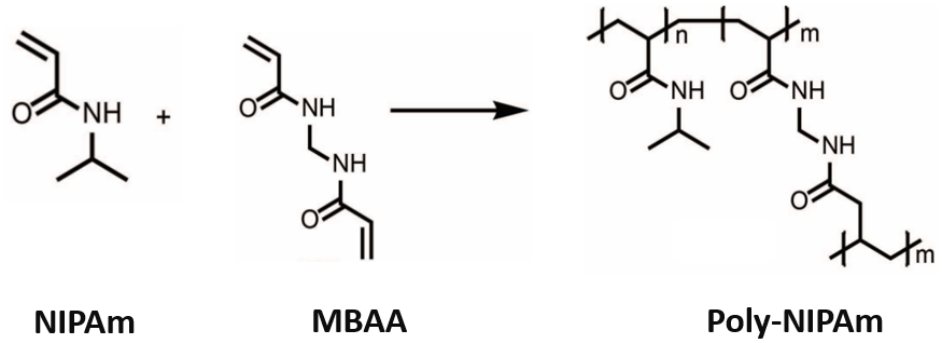

Figure 4.1. Synthesis schematic of poly-NIPAM hydrogel from NIPAm monomer and MBAA crosslinker (adapted from [81]).

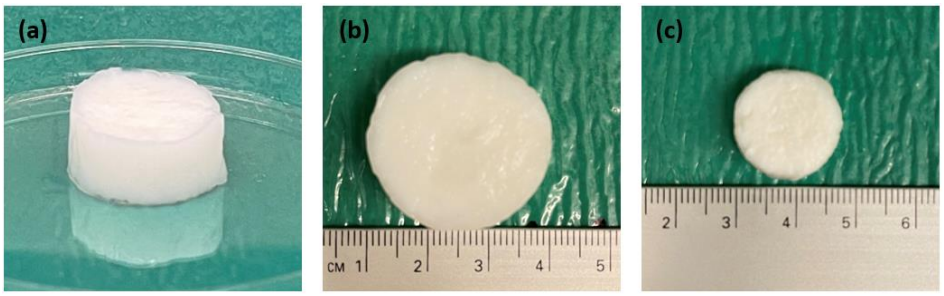

Figure 4.2. Digital photos of room temperature synthesized poly-NIPAm hydrogel: **(a)** equilibrium state of hydrogel; **(b)** at 25℃; and **(c)** at 40℃ after 2 hrs water retention test.

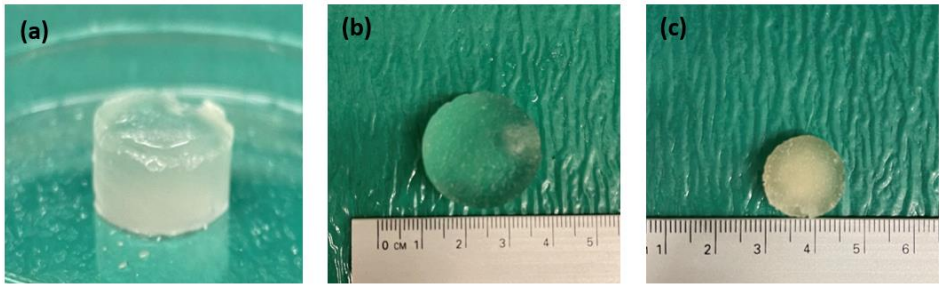

Figure 4.3. Digital photos of low temperature synthesized poly-NIPAm hydrogel: **(a)** equilibrium state of hydrogel; **(b)** at 25℃; and **(c)** at 40℃ after 2 hrs water retention test

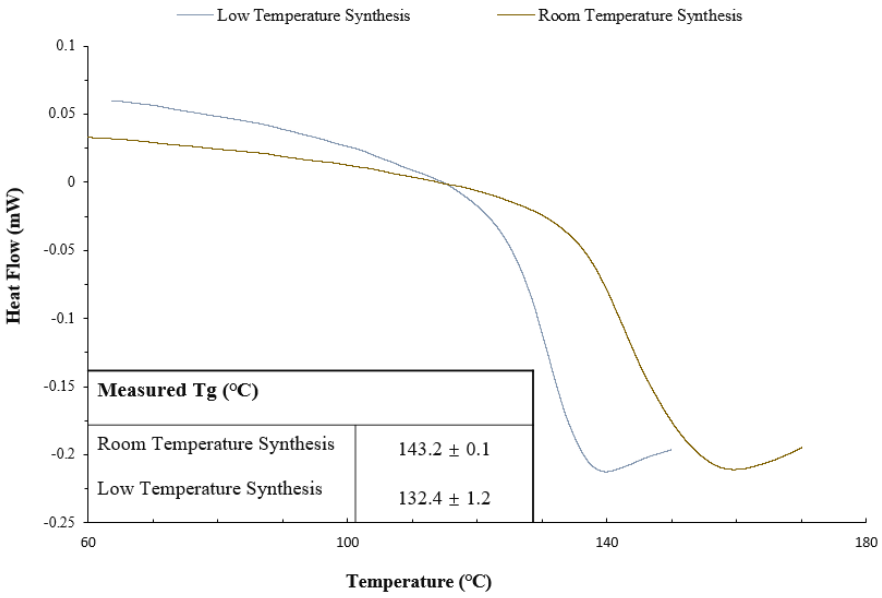

Figure 4.4. DSC thermograms of poly-NIPAm hydrogels

Figure 4.4 depicts the glass transition temperature of the two poly-NIPAm hydrogels. The room temperature synthesized poly-NIPAm hydrogel usually provides a microporous structure gel network, while the low temperature synthesis fabricates the macroporous structure. Therefore, microporous one has a larger Tg value as what was discussed in ref [82]. Owing to the porosity of each hydrogel samples that has an impact on the glass transition temperature, therefore, the Tg value decreases with the increased porous distribution.

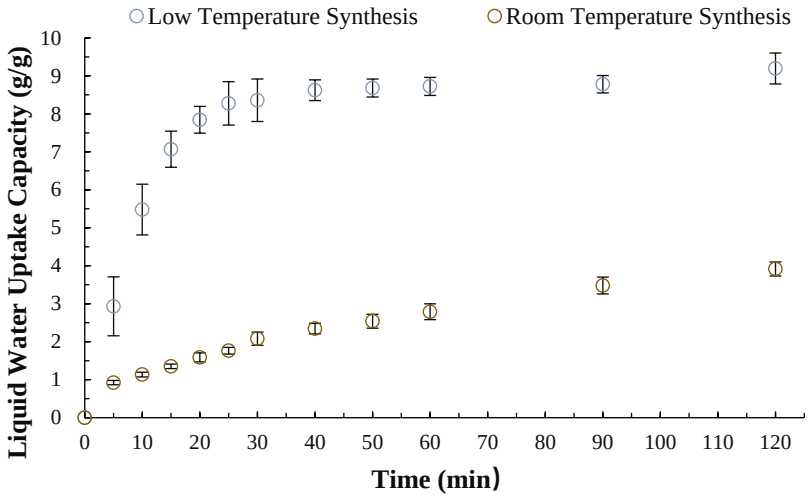

Figure 4.5. Plots of swelling kinetics of poly-NIPAm hydrogels

Preparation Method	Water Uptake after 2 hrs (g/g)	Equilibrated Water Uptake (g/g)
Room Temperature	3.92 ± 0.18	6.23 ± 0.69
Low Temperature	9.19 ± 0.41	9.22 ± 0.43

Table 4.1. Liquid water uptake capacity of poly-NIPAm hydrogels: Equilibrated water uptakes were measured after 5 days immersing in the liquid water.

Figure 4.5 summarizes the swelling kinetics curve of the two different synthesized poly-NIPAm hydrogels at room temperature as a function of time. Liquid water uptake capacities are directly calculated based on their swelling ratio after incubating into pure water. The vast difference between the two methods is visible in Table 4.1, which summarizes the liquid water uptake capacities of these two hydrogels measured after two hours of swelling tests. The low temperature synthesized sample presents the maximum uptake at 9.19 ± 0.41 g/g; meanwhile, the room temperature synthesized sample shows the weight change of 3.92 ± 0.18 g/g after 2 hours of contact with liquid water. As seen in Figure 4.5, at approximately 25 minutes, low temperature synthesized poly-NIPAm

hydrogel starts to approach the equilibrium state and attains its saturated liquid water content around 40 minutes. The main reason for different liquid water uptake performances is the pore morphology and wall thickness [83]. The room temperature synthesis method produces the conventional gels, which only contain smaller interconnected porous networks. Besides, the distance between pores within conventional hydrogel is much longer than the cryogel from low temperature synthesis due to the denser network structure and thicker walls of pores. On the contrary, cryogels show larger porous with thinner walls that bring up a faster and more significant liquid water uptake across the macroporous structure [68, 83].

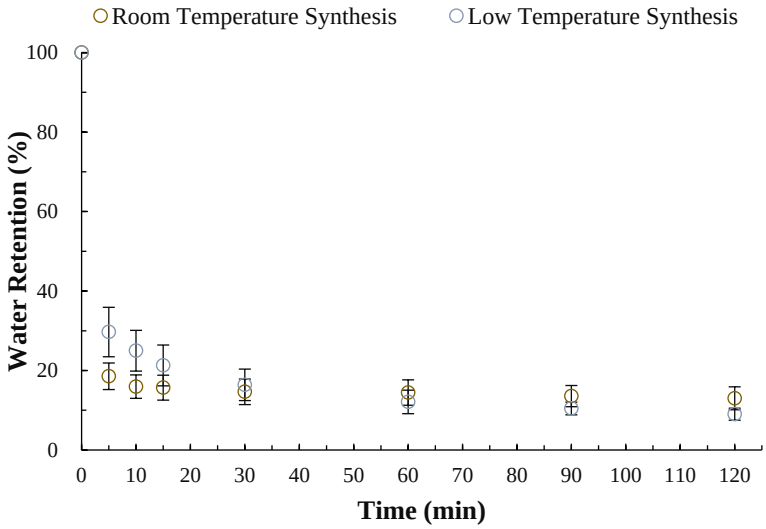

Figure 4.6. Plots of deswelling kinetics of synthesized poly-NIPAm hydrogels

Sample	Water Retention (%)
Room Temperature Synthesis	13.0 ± 2.9
Low Temperature Synthesis	9.0 ± 1.5

Table 4.2. Water retention of poly-NIPAm hydrogels at 40 ℃ water after 2 hrs tests

Figure 4.6 manifests the deswelling kinetics of poly-NIPAm hydrogels as a function of time at 40℃ water bath from the water retention test. In the y-axis of the plot, water retention represents the amount of water that hydrogels can retain in the matrix after immersing in an elevated temperature environment in which go above its LCST. As aforesaid, poly-NIPAm hydrogel undergoes a volume phase transition, from hydrophilic to hydrophobic, when the temperature is higher than its LCST. Therefore, the water retention value could reflect the releasing behavior and retaining ability of poly-NIPAm hydrogels. Furthermore, it provided the direct reference for structural designs of the hydrogel-based desiccant for AWE technology because the hydrogel matrix functions as a ‘reservoir’ in the designed system. In Figure 4.6, both poly-NIPAm hydrogels exhibit moderate and comparable releasing behavior; they all reached the releasing equilibrium state within the first hour of the test.

As Table 4.2 summarizes, the equilibrium water retention of room temperature synthesized poly-NIPAm is 13.0 ± 2.9 %. The two comparisons of (b) and (c) in Figure 4.2 and Figure 4.3 are the explicit pictorial demonstrations of the thermoresponsiveness of the hydrogels. Notably, the room temperature synthesized gel had faster kinetics at the initial deswelling stage compared to the other, a phenomenon that Zhang and colleagues previously explained. They deduced that the unexpected smaller shrinking of the hydrogel was potentially from its oriented and regular highly porous structure [84]. Such a structure might be unable to collapse at a similar level as the room temperature synthesized hydrogel.

As mentioned earlier, the low temperature synthesis method was adopted to prepare the macroporous structure hydrogel with 0.1 to 1 μm pore size. In contrast, the pore size of microporous hydrogel is usually 0.01 to 0.1 μm [68,69]. The comparison results from above verified the effect of the porous structure on the swelling kinetics of the hydrogel. The opening porosity and pore structure of the hydrogel significantly influenced the equilibrated water uptake capacity. Furthermore, the low temperature synthesis method changes pore size, which provides more internal free space for capturing the water than the usual room temperature synthesis method. Consequently, the low temperature synthesis method was adopted as the way to prepare hydrogel.

4.1.2 Effect of Chemical Composition

As shown in Figure 4.7 to Figure 4.9, the hydrogels retained similar appearance from the visual observation; however, a relationship was revealed, as the appearance of samples became less transparent with a decrease in monomer concentration. Such a subtle appearance change could be attributed to the different chemical compositions of the gel matrix. The molar ratio of crosslinker and monomer might affect the crosslink density of hydrogel samples. Therefore, sample 3 possess the lowest initial monomer concentration, which could represent the highest crosslinking concentration to result in the least transparent morphology.

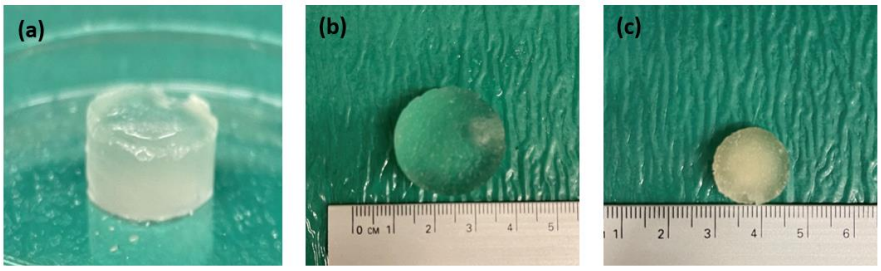

Figure 4.7. Digital photos of sample 1: **(a)** equilibrium state of hydrogel; **(b)** at 25°C; and **(c)** at 40°C after 2 hrs water retention test

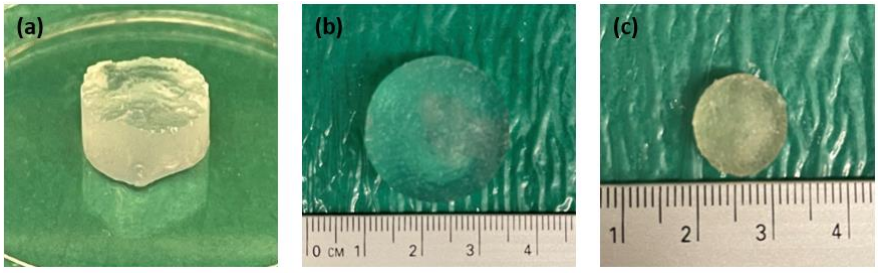

Figure 4.8. Digital photos of sample 2: **(a)** equilibrium state of hydrogel; **(b)** at 25°C; and **(c)** at 40°C after 2 hrs water retention test

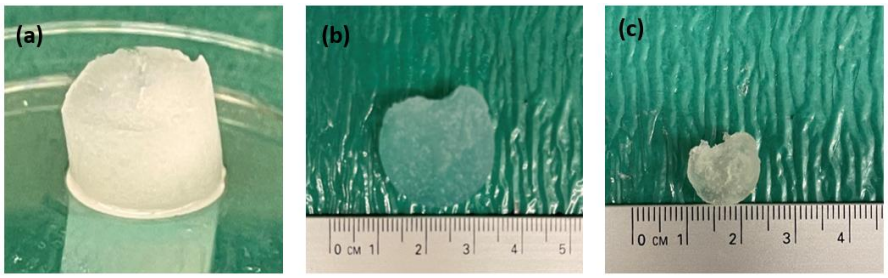

Figure 4.9. Digital photos of sample 3: **(a)** equilibrium state of hydrogel; **(b)** at 25°C; and **(c)** at 40°C after 2 hrs water retention test

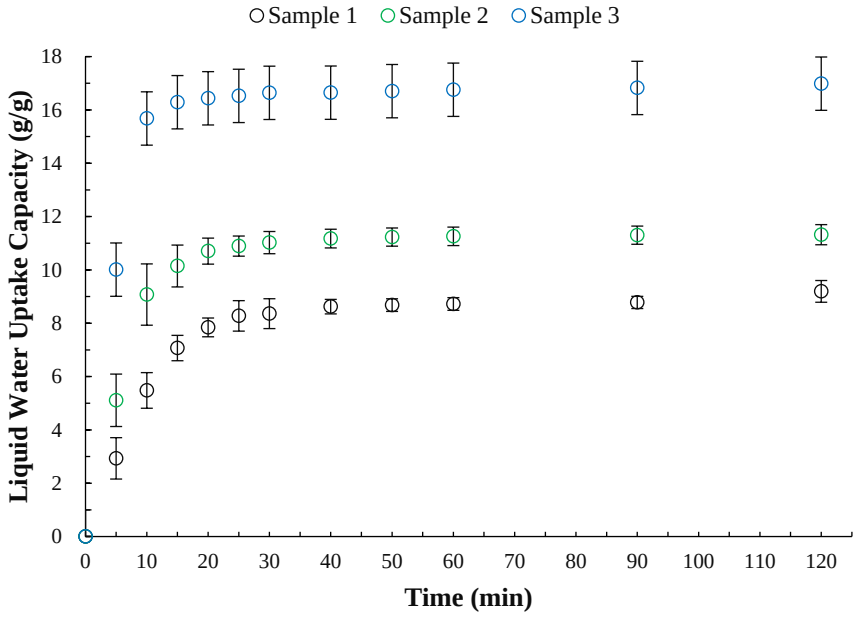

Figure 4.10. Plots of swelling kinetics of low temperature synthesized poly-NIPAm hydrogels

Poly-NIPAm Hydrogels	Water Uptake Capacity after 2 hrs (g/g)	Equilibrated Capacity (g/g)
Sample 1	9.19 ± 0.41	9.22 ± 0.43
Sample 2	11.32 ± 0.38	11.4 ± 0.42
Sample 3	16.98 ± 1.26	17.02 ± 1.25

Table 4.3. Liquid water uptake capacity of low temperature synthesized poly-NIPAm hydrogels with various ratio of crosslinker/monomer: Equilibrated water uptakes were measured after 5 days immersing in the liquid water.

Apart from the influence of the synthesis temperature and porous structure, the effect of chemical composition, initial monomer concentration on swelling kinetics of the hydrogel was also computed by liquid water uptake and water retention tests. Figure 4.10 shows the liquid water uptake capacities of these hydrogels from the swelling tests. It appeared that the liquid water uptake capacities of hydrogels vary with the monomer concentration in the gel system. The liquid water uptake rate of poly-NIPAm hydrogels also presents a clear difference among the three hydrogel samples. Sample 3 started to reach the equilibrium after fifteen minutes, 5 minutes, and 10 minutes faster than sample 2 and sample 3, respectively. The effect of the monomer concentration is displayed in Figure 4.10 that the lower monomer concentration makes for higher liquid water uptake equilibrium capacity and faster kinetics at room temperature. Such an inverse relationship between the monomer concentration and the swelling ratio was also previously reported in other cryogels [85,86].

The previous work illustrated that the conventional hydrogel from the room temperature synthesis method with a lower crosslinker concentration would result in a higher swelling ratio [80]. Such a phenomenon occurs because a lower crosslinker concentration caused the lower crosslinking density, which provides enough free space inside the gel matrix that quickly makes the gel expand for water molecules storage. In contrast, the higher crosslinking density usually creates a denser network in the gel, which impedes the water molecules from diffusing within the gel matrix.

Interestingly, from the liquid water uptake test results in Figure 4.10, the higher crosslinking density had the best liquid water uptake capacities, exactly an inverse proportion compared to the conventional hydrogel from the room temperature synthesis method. The probable reason may be based on two previous findings. Firstly, the crosslinker level, MBAA, used in low temperature hydrogel synthesis method, will not cause the distinct pore size change [87,88]. Secondly, monomer concentration in the synthesized hydrogel system is related to the pore size and the wall thickness. With an increased monomer concentration, pore size becomes smaller, leading to a lower swelling ratio [83,89]. Since the porosity of gel impacted the swelling ratio, and crosslinker level will not influence pore size, it can be assumed that the amount of crosslinker used for three low temperature synthesis hydrogels is not a determining factor. These previous findings could explain the appearance of the inverse relation between monomer concentration and liquid water uptake capacity obtained through this study.

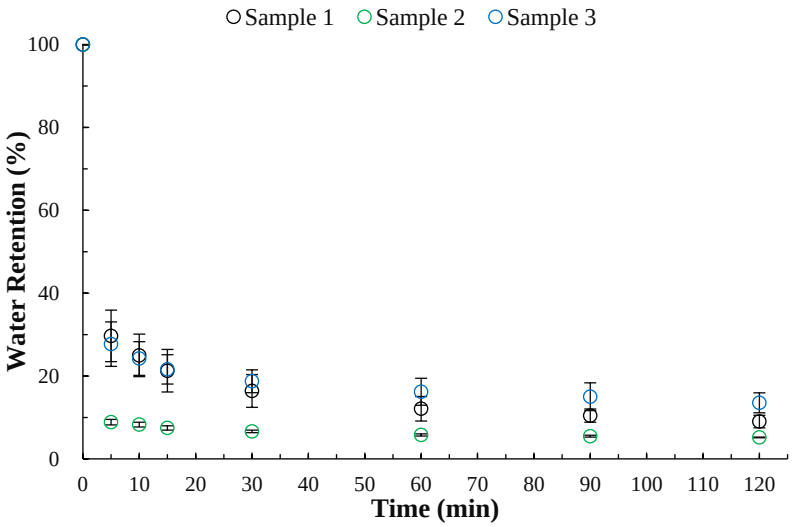

Figure 4.11. Plots of deswelling kinetics of three low temperature synthesized poly-NIPAm hydrogels

Poly-NIPAm Hydrogels	Water Retention (%)
Sample 1	9.00 ± 1.5
Sample 2	5.20 ± 0.1
Sample 3	13.5 ± 2.4

Table 4.4. Water retention of low temperature synthesized poly-NIPAm hydrogels at 40℃ water after 2 hrs tests.

Figure 4.11 displays the deswelling kinetic curves of samples in a 40 ℃ water bath from the water retention tests. For the deswelling performance, samples reached equilibrium within 60 minutes. Sample 2 had the fastest kinetics, and sample 3 was the lowest. The water retention capacity of sample 1 had a median value when compared with other samples. Frankly, it is uncommon to lack a clear relationship between the monomer concentration and the deswelling behavior of the low temperature synthesized hydrogel. As previously proved, the lower the monomer concentration will lower the water retention capacity [83,84]. The possible reason for this non-linear relationship may

involve that the temperature at which the monomer solution was degassed and at which gelation was started might not be well agreed upon due to experimental errors. Therefore, the inner macroporous structure of samples did not form consistently, resulting in an unconformable deswelling behavior. Nevertheless, sample 3 released about 14.72 g of captured water after 2 hours of water retention test, benefiting from superior liquid water uptake capacity. The poly-NIPAm hydrogel with the lowest monomer concentration was selected as the most efficient composition for the following task.

4.2 Integration of Optimized Poly (*N*-Isopropylacrylamide) Hydrogel with Hygroscopic Materials

4.2.1 Synthesis of Gel Desiccants

Figure 4.12 is the schematic diagram of each gel desiccant. As shown, poly-NIPAm and poly-VIM gel desiccants were all homopolymeric hydrogels made from a single crosslinked monomer. The poly (VIM-co-NIPAm) were formed from both VIM and NIPAm monomers. The IPN gel desiccant was one of the multi-polymeric hydrogels formed from two independent polymers where at least one is crosslinked [90]. As usual, interpenetrating polymeric network hydrogels possess a superior property to each of the single polymers in their system [90].

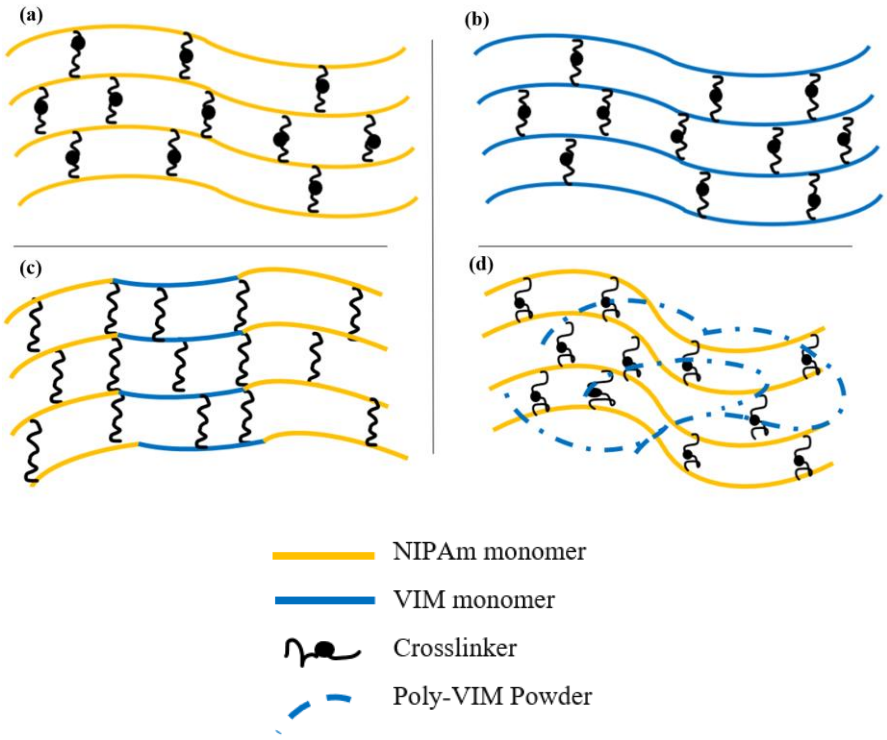

Figure 4.12. Schematic of gel desiccants: **(a)** poly-NIPAm; **(b)** poly-VIM; **(c)** poly (VIM-*co*-NIPAm); and **(d)** poly-VIM/poly-NIPAm IPN

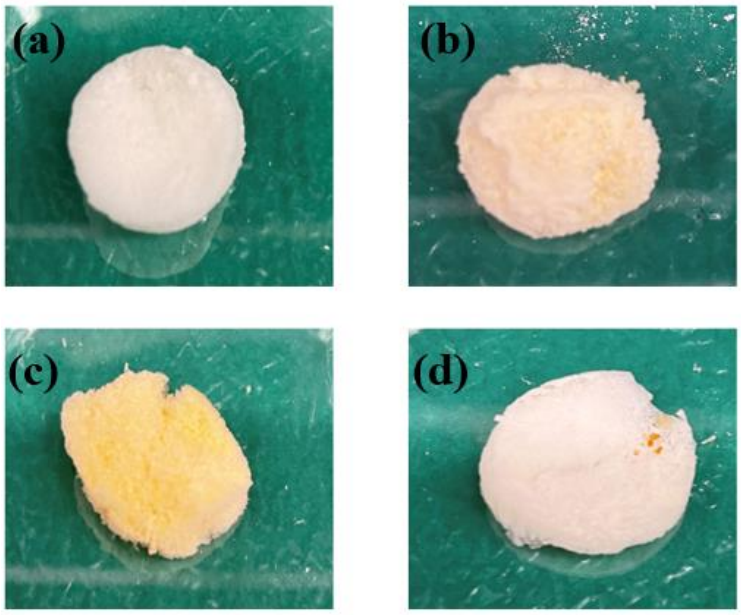

Figure 4.13. Digital photographs of gel desiccants: **(a)** poly-NIPAm; **(b)** poly-VIM; **(c)** poly (VIM-*co*-NIPAm); and **(d)** poly-VIM/poly-NIPAm IPN

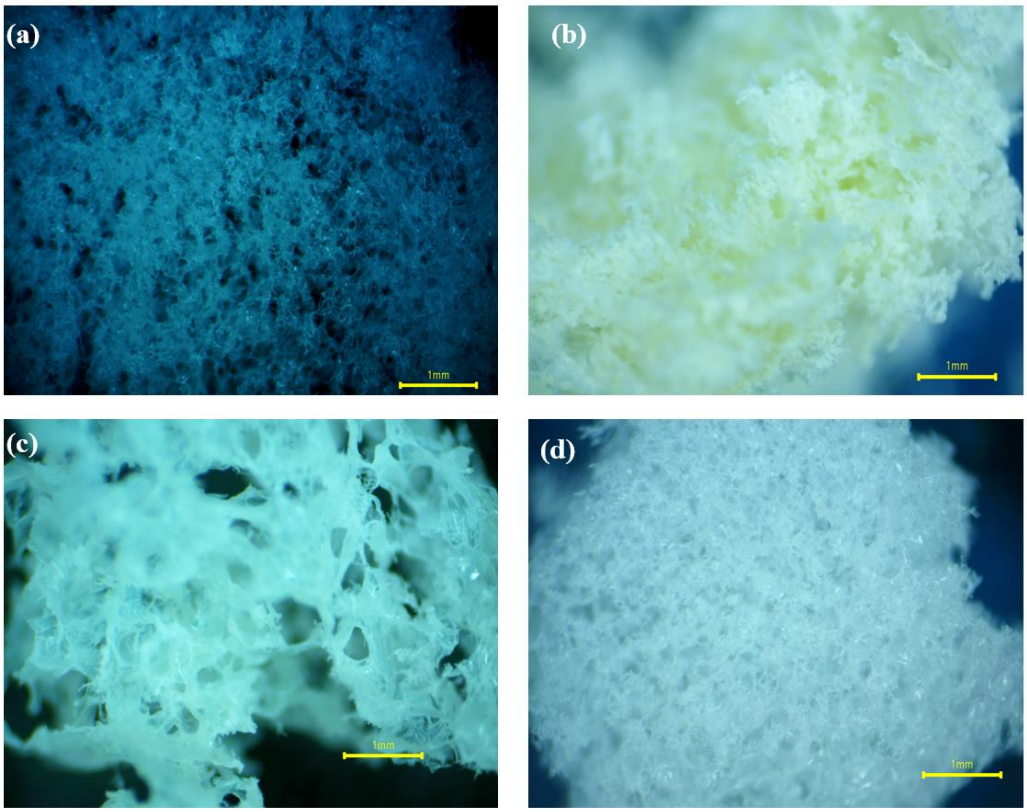

Figure 4.14. Optical microscope photographs of gel desiccants: **(a)** poly-NIPAm; **(b)** poly-VIM; **(c)** poly (VIM-*co*-NIPAm); and **(d)** poly-VIM/poly-NIPAm IPN

Figure 4.13 gives the visual observation of each gel desiccant at a freeze-dried state. All gel desiccants were synthesized using low temperature synthesis, and further freeze-drying was implanted to preserve the pore structure. Such a combination gave gel desiccants a sponge-like morphology. The optical microscope photographs of gel desiccants in Figure 4.14 did not drastically indicate the differences in pore size. Nevertheless, they express that low temperature synthesis and freeze-drying contribute to the porosity. The presence of these pores provides the internal channels where the moisture from the air may easily be captured.

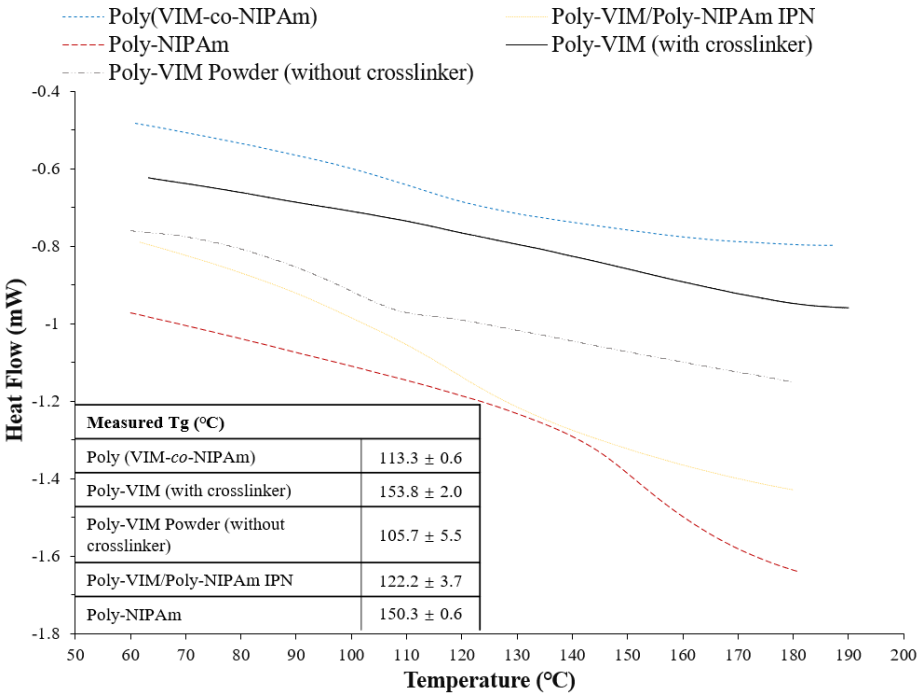

Figure 4.15. DSC thermograms of gel desiccants

The glass transition temperatures (Tg) of each gel desiccant are summarized in the insert table in Figure 4.15. Since glass transition temperature is deemed one of the value criteria to study the thermophysical property of a polymer network, it is usually utilized to determine the miscibility, compatibility, and even the role of each component in a polymer network [91]. As seen in Figure 4.15, with an insert table of the Tg values, each gel desiccant shows the single endothermic phase transition values. These data help to manifest the formation of the network. Ribellies *et al* [92] advises that if a polymer network has a single phase-transition peak, this indicates the successful formation of the cross-linked IPN network. More specifically, the Tg value of IPN gel desiccant was in the intermediate between its neat constituent parts, which is also a precise indication of the formation [91, 93].

4.2.2 Effect of Network Structure on Moisture Uptake

All gel desiccants are retrieved from the vial after thawing and cut into four pieces of the same thickness and diameter for freeze-drying. Later, the freeze-dried gel samples were placed on the petri dish bottom in the humidity hood, as shown in Figure 3.1. Figure 4.16 (a) and (b) summarize the moisture uptake performance of each gel desiccants at the given time within 2 hours normalized by the weight change and surface area approaches. Pure poly-VIM and pure poly-NIPAm gel desiccants were used as the control samples reflecting the features of the homopolymeric gel network for moisture uptake. Interestingly, the pure poly-NIPAm gel desiccant was preparaed using low temperature synthesis, and the freeze-drying combination also showed moisture uptake capability, which is also described in the ref [14].

Nevertheless, the homopolymeric gel desiccants are not suited enough to capture and store moisture from the air. The copolymeric gel desiccant shows better moisture uptake performance after introducing a hygroscopic polymer into the designed gel system. As a result, copolymeric gel desiccant starts approaching the equilibrium and reaches the maximum capacities of 0.177 ± 0.004 g/g. As shown in Figure 4.16 (a), the orange color represents the moisture uptake of poly-VIM/poly-NIPAm IPN gel desiccant. It attained maximum moisture uptake capacity in a shorter time and exhibits the relative better performance compared to the others.

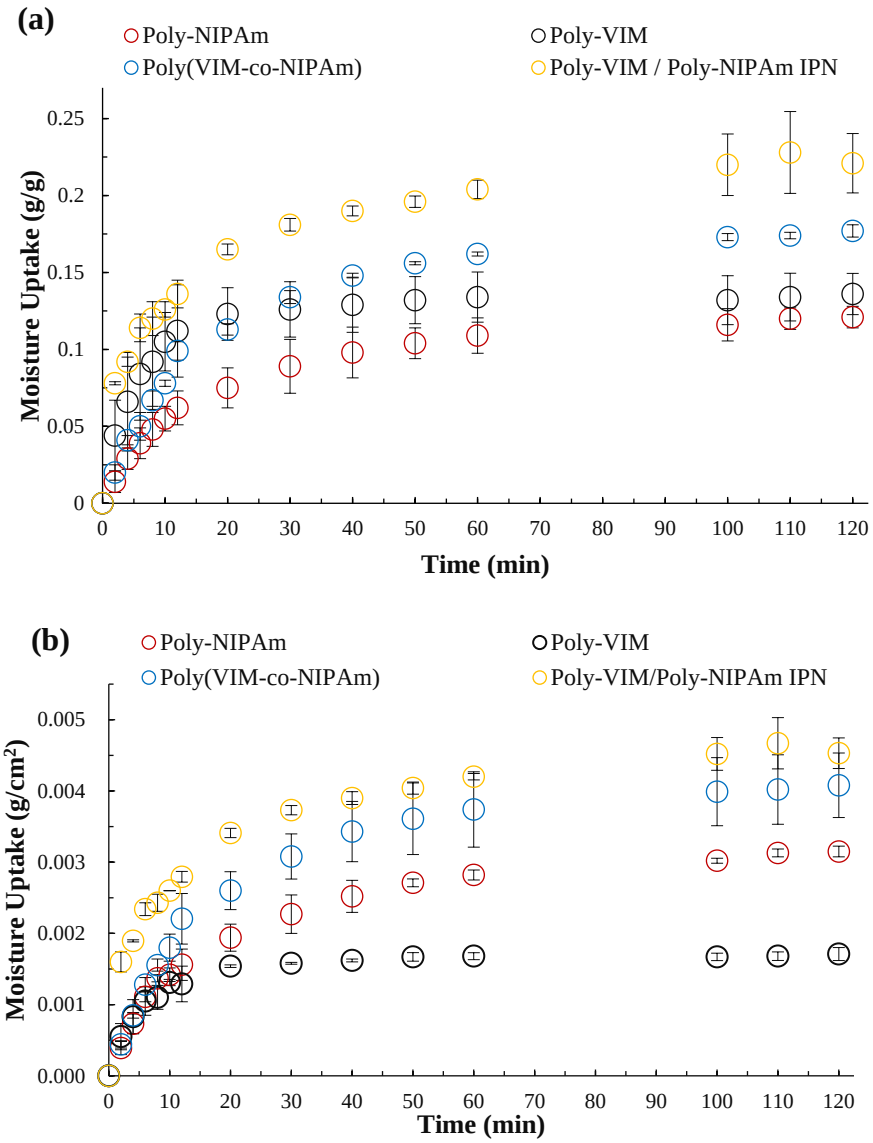

Figure 4.16. The moisture uptake results of gel desiccants at 24°C and 60% RH: **(a)** normalized by weight change, and **(b)** normalized by surface area.

(a)

Gel Desiccant Samples	Maximum Capacity (g/g)
Poly-VIM/Poly-NIPAm IPN	0.228 ± 0.027
Poly (VIM-co-NIPAm)	0.177 ± 0.004
Poly-VIM	0.136 ± 0.013
Poly-NIPAm	0.121 ± 0.007

(b)

Gel Desiccant Samples	Maximum Capacity (g/cm^2)
Poly-VIM/Poly-NIPAm IPN	0.00453 ± 0.00022
Poly (VIM-co-NIPAm)	0.00408 ± 0.00045
Poly-VIM	0.00171 ± 0.00009
Poly-NIPAm	0.00315 ± 0.00008

Table 4.5. The maximum capacity of gel desiccants after 2 hrs moisture uptake test at 24℃ and 60% RH. The results were calculated as the average of two tests: **(a)** normalized by weight change, and **(b)** normalized by surface area.

Figure 4.16 (b) and Table 4.5 (b) are about the moisture uptake test results normalized by the surface area approach. All gel desiccant samples were made into a disk-like shape and the net surface area contact with the humid air was calculated using the surface area formula of the cylinder. Similarly, two composite gel desiccants are comparable and showed better moisture uptake performance than that of homopolymeric gel desiccants. Therefore, composite gel desiccant with IPN structure is suggested that is more suitable for moisture uptake.

It is worth noting that the curve trends of the two homopolymeric gel desiccants normalized by surface area are reversed compared to that of were normalized by weight change. The potential reason for such a situation is that the poly-VIM gel desiccant becomes lighter after the sublimation during the drying process in the freeze dryer. The

hydrogel matrix of poly-VIM gel desiccant might not be crosslinked enough due to a lower molar ratio of crosslinker to monomer. Therefore, the low temperature synthesis method produces a soft and brittle three-dimensional network. On the other hand, the thawed gel desiccant sample might contain a certain amount of frozen liquid inside the matrix, followed by sublimating thoroughly during the drying process, which also resulted in the lighter weight. Moreover, the freeze-drying process requires all samples to be frozen first, which means that immersing into water before freezing solid may cause sample loss. Consequently, the freeze-dried weight of poly-VIM gel desiccant is smaller than that of the gel desiccants. In the end, the curve trends of the two approaches results in different versions.

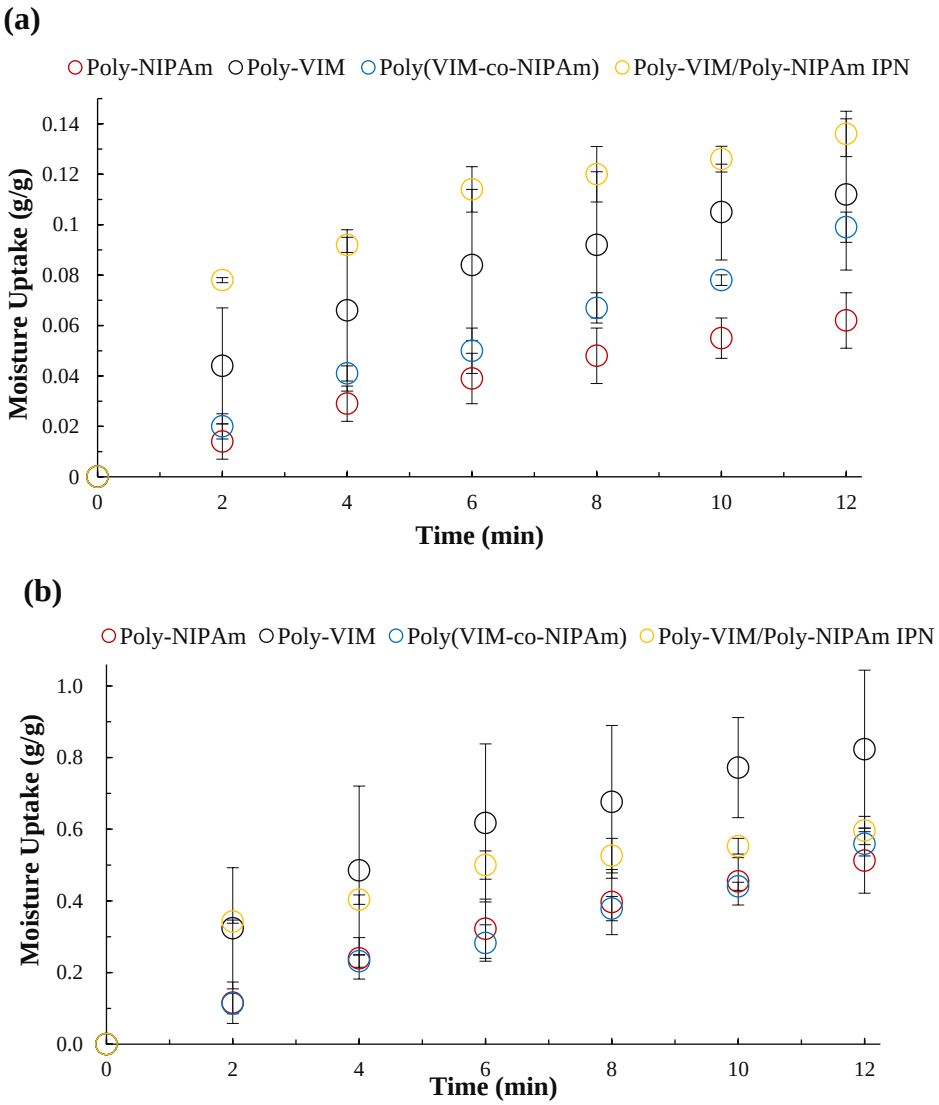

Figure 4.17. The moisture uptake results of gel desiccants at 24℃ and 60% RH normalized by weight change: **(a)** the initial stage of moisture uptake results from 0 to 12 minutes, and **(b)** the initial stage of moisture uptake results normalized by maximum capacity.

(a)

Time (min)	Poly-NIPAm	Poly-VIM	Poly(VIM-*co*-NIPAm)	Poly-VIM/Poly-NIPAm IPN
0	0	0	0	0
2	0.014 ± 0.007	0.044 ± 0.023	0.020 ± 0.005	0.078 ± 0.001
4	0.029 ± 0.007	0.066 ± 0.032	0.041 ± 0.003	0.092 ± 0.003
6	0.039 ± 0.010	0.084 ± 0.030	0.050 ± 0.009	0.114 ± 0.009
8	0.048 ± 0.011	0.092 ± 0.029	0.067 ± 0.006	0.120 ± 0.011
10	0.055 ± 0.008	0.105 ± 0.019	0.078 ± 0.002	0.126 ± 0.005
12	0.062 ± 0.011	0.112 ± 0.030	0.099 ± 0.006	0.136 ± 0.009

(b)

Time (min)	Poly-NIPAm	Poly-VIM	Poly(VIM-*co*-NIPAm)	Poly-VIM/Poly-NIPAm IPN
0	0	0	0	0
2	0.116 ± 0.058	0.324 ± 0.169	0.113 ± 0.028	0.342 ± 0.004
4	0.240 ± 0.058	0.485 ± 0.235	0.232 ± 0.017	0.404 ± 0.013
6	0.322 ± 0.083	0.618 ± 0.221	0.282 ± 0.051	0.500 ± 0.039
8	0.397 ± 0.091	0.676 ± 0.213	0.379 ± 0.034	0.526 ± 0.048
10	0.455 ± 0.066	0.772 ± 0.140	0.441 ± 0011	0.553 ± 0.022
12	0.512 ± 0.091	0.824 ± 0.221	0.559 ± 0.034	0.596 ± 0.039

Table 4.6. The moisture uptake results of gel desiccants at 24℃ and 60%. The results were calculated as the average of two tests and normalized by weight change: **(a)** weight change of gel desiccants from 0 to 12 minutes, and **(b)** weight change of gel desiccants from 0 to 12 minutes normalized by maximum capacity.

To understand the adsorption kinetics of these gel desiccants, the initial stage of the moisture uptake performance was further focused and investigated, as shown in Figure 4.17, which was normalized by the weight change approach. Figure 4.17 (a) displayed that the initial adsorption performance of gel desiccant samples followed similar trends. In consequence, the initial stage of moisture uptake results was normalized by the plateau (maximum adsorption capability). Specifically, the raw data of each gel desiccant from Figure 4.17 (a) was divided by its maximum adsorption capacity, summarized in Figure 4.17 (b). Since each gel desiccant was synthesized under identical conditions except for their gel network structure, Figure 4.17 (b) suggested that different structures may lead to variable moisture adsorption kinetics. Due to the significant and overlapping error bars of the experimental data, no empirical model fitting was performed for each gel desiccant.

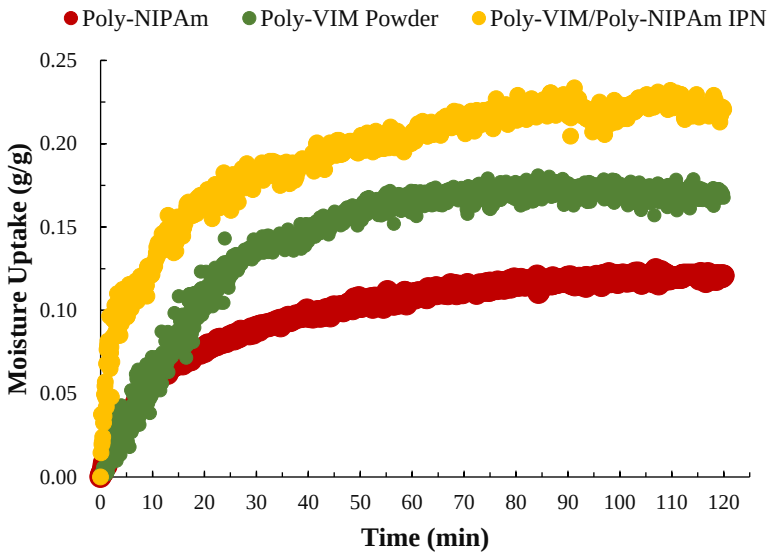

Figure 4.18. The moisture uptake results of IPN gel desiccant and its constituents parts at 24℃ and 60% RH normalized by weight change.

In the IPN system, the poly-VIM powder is an uncrosslinked phase, while the poly-NIPAm hydrogel is a crosslinked phase. Figure 4.18 is a straightforward representation of how each component in the IPN gel desiccant system contributes to its moisture uptake. After merging the hygroscopic powder into a hydrogel matrix, the adsorbed moisture from humid air can be transported into the gel matrix. It reveals that the IPN gel desiccant showed a synergistic function. That structural unit can be further rationally regulated with other materials to possess more desired features.

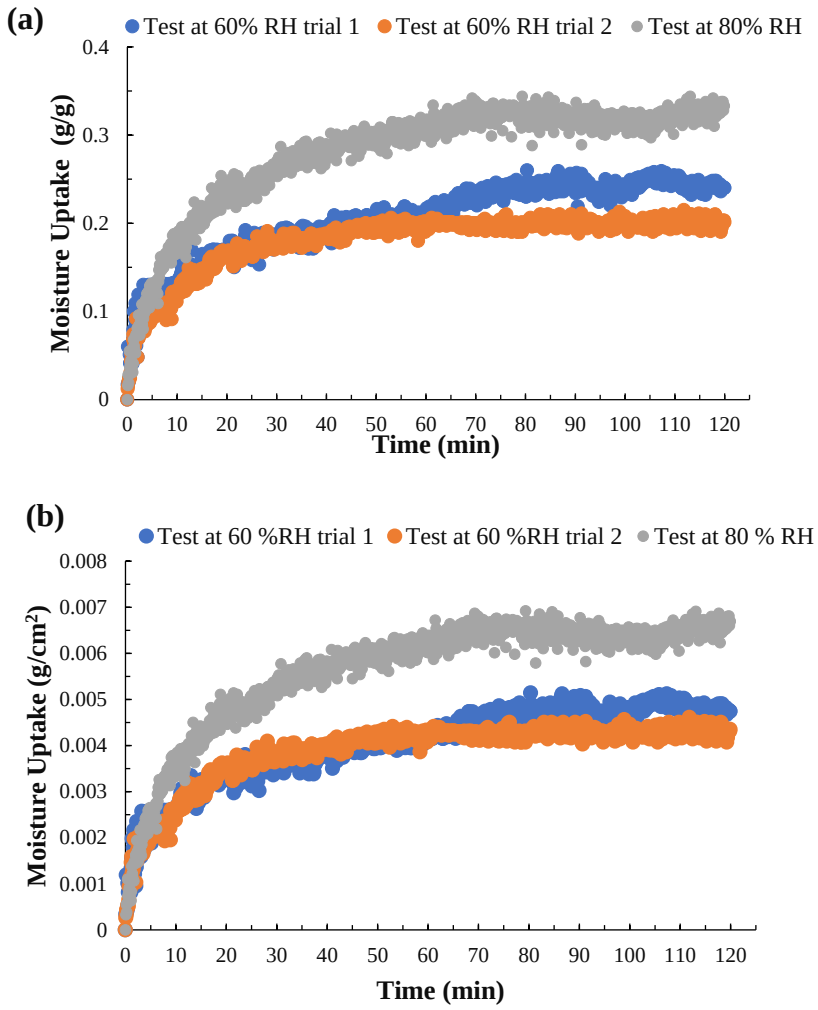

Figure 4.19. The moisture uptake results of IPN gel desiccants at 24℃ and different humidity conditions: **(a)** normalized by weight change; **(b)** normalized by surface area.

Figure 4.19 demonstrates that the interpenetrating polymeric network structure functions adequately and captures more humid air in a higher relative humidity environment. Das suggests that copolymeric hydrogel usually enlarges the swelling ability of hydrogel; it could also compromise the gel's mechanical properties due to the presence of at least one hygroscopic monomer within its matrix [90]. Conversely, regarding the difference between the two network structures of composite gel desiccants, the hydrogel with interpenetrating polymeric network structure comprises two partially

interlaced phases on the molecular scale view, thereby improving the mechanical property. It has a denser gel matrix that produces a stiffer characteristic and a tougher mechanical property [78,90]. A solid three-dimensional network structure is the prerequisite to achieve multiple capture-release cycles to increase the efficiency of AWE technology.

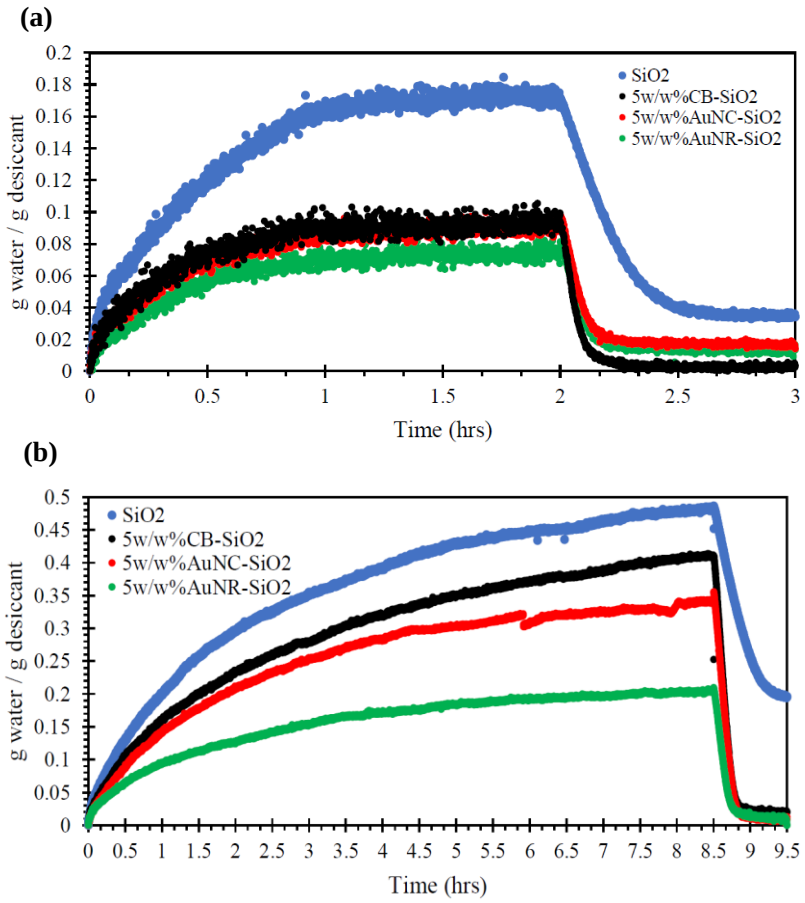

Figure 4.20. The moisture uptake and desorption test results of bare SiO_2-based particle desiccants at room temperature: **(a)** 60% RH and **(b)** 80% RH (adapted from [94])

Particle Desiccant Samples	Maximum capacity (g/g)
SiO_2	0.201 ± 0.0152
5w/w%CB-SiO_2	0.119 ± 0.0083
5w/w%AuNC-SiO_2	0.116 ± 0.0156
5w/w%AuNR-SiO_2	0.101 ± 0.0059

Table 4.7. The maximum capacity of particle desiccants (g/g) at 60 % RH (adapted from [94])

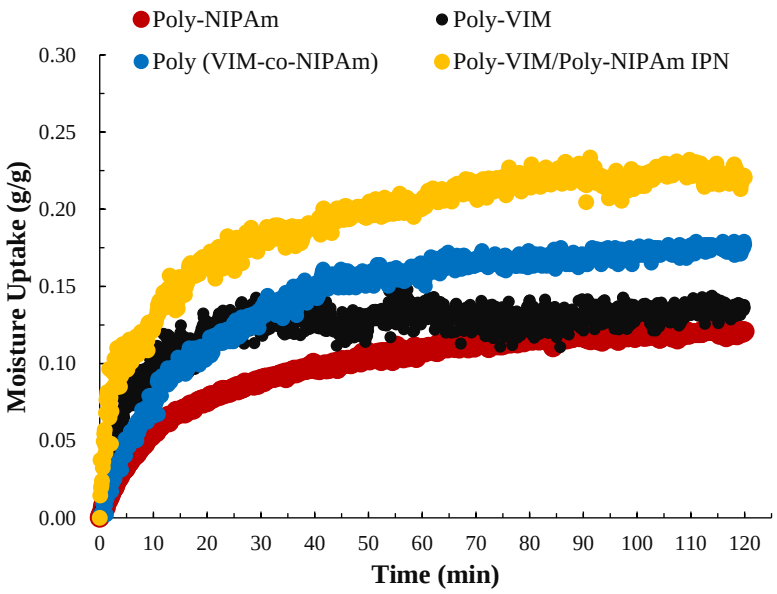

Figure 4.21. The curves of moisture uptake test results of each gel desiccants at 24℃ and 60% RH normalized by weight change.

Mulchandani and colleagues determined the hygroscopicity of a series of SiO2 based photothermal particle desiccants [94]. For the moisture uptake tests, they first weighted out the one gram of particle desiccant samples on the petri dish and placed them in the humidity chamber as shown in Figure 3.1 to record the weight change after contacting the humid air. Figure 4.20 and Table 4.7 summarized the moisture uptake performances of each SiO2-based desiccant at 60% RH by weight change normalization. All particles desiccants attained the equilibrium state and maximum uptake capacity

within 2 hours. The gel desiccant samples from the thesis work had comparable moisture uptake performance than the particle desiccants based on the maximum capacities, as Figure 4.21 and Table 4.5 depicts. Composite gel desiccant with interpenetrating polymeric network displayed the best moisture uptake. However, it is worth noting that particles desiccants possess different morphology, which resulted in the surface areas. Table 4.8 shows the specific surface areas of each particle desiccant determined by BET surface area analysis. The moisture uptake curve trends of gel desiccants normalized by surface areas are given in Figure 4.22. The surface areas of the bulk gel desiccants are roughly calculated using the surface area formula of the cylinder that might not be necessarily precise enough to be used to compare to particles desiccants for their hygroscopicity.

Desiccant	BET Surface Area (m^2/g)
SiO_2	459.2
SiO_2-APTES	289.2
5wt%CB-SiO_2	297.2
5wt%AuNC-SiO_2	281.3
5wt%AuNR-SiO_2	248.6

Table 4.8. BET surface areas of particle desiccants (adapted from [94]).

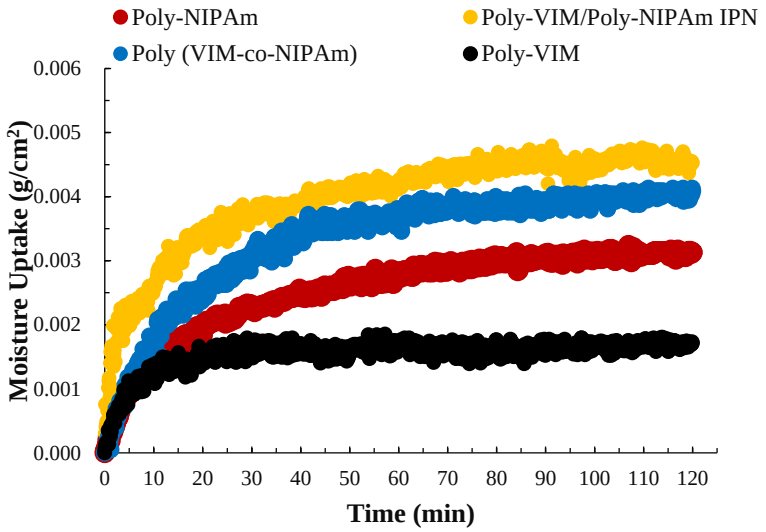

Figure 4.22. The curves of moisture uptake test results of each gel desiccants at 24℃ and 60% RH normalized by surface area.

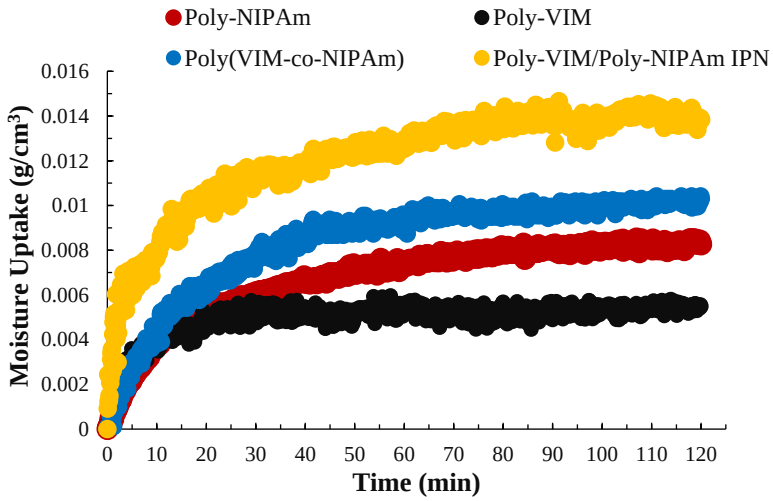

Figure 4.23. The curves of moisture uptake test results of each gel desiccants at 24℃ and 60% RH normalized by volume.

Gel Desiccant Samples	Maximum Capacity (g/cm³)
Poly-VIM/Poly-NIPAm IPN	0.014659 ± 0.00249
Poly (VIM-co-NIPAm)	0.010421 ± 0.00063
Poly-VIM	0.005959 ± 0.00072
Puoly-NIPAm	0.068530 ± 0.00039

Table 4.9. The maximum capacity of gel desiccants after 2 hrs moisture uptake test at 24℃ and 60% RH. The results were calculated as the average of two tests and normalized by volume.

Since the gel desiccants are all disk-like morphology in the cylinder shape, the volume of the bulk part of hydrogel is another parameter to evaluate the moisture uptake performances. Figure 4.23 and Table 4.9 summarize the moisture uptake performance of gel desiccants normalized by volume approach, roughly calculated using the volume formula of the cylinder. From such an analysis method, the gel desiccants with IPN structure still showed the best capacity. Significantly, a more accurate characterization for the porosity and surface area of bulk gel desiccants and a precise comparison between the thesis work's desiccants and previous work will be completed shortly.

CHAPTER 5

SUMMARY AND FUTURE DIRECTION

5.1 Summary

This study elucidated using the low temperature synthesis method to fabricate a series of hydrogel-based highly porous desiccants for AWE technology. These hydrogel-based porous desiccants with different structures were also utilized to systematically investigate how porous and network structures affect moisture uptake performance.

First, we focused on tuning the synthesis parameters to optimize poly-NIPAm hydrogel's ability to store water molecules from the humid air. The first parameter we investigated was controlling the temperature of the synthesis method. The low temperature synthesized poly-NIPAm hydrogel performed the better liquid water uptake capacity. The second approach we researched was tuning the initial monomer concentration used in gel synthesis. The work showed that the poly-NIPAm hydrogel with a higher swelling ratio was realized by decreasing the initial monomer concentration. Therefore, the low temperature synthesis method with lower monomer concentration was kept as the basis for developing hydrogel-based porous desiccants summarized below.

Second, we incorporated the vinyl imidazole into the optimized poly-NIPAm hydrogel. A series of vinyl imidazole-contained gel desiccants were synthesized using the low temperature synthesis method. By implementing moisture uptake tests, gel desiccant with IPN structure showed larger moisture uptake capacity and faster-capturing kinetics than other gel desiccant samples within the first two hours. Such an IPN gel desiccant

system showcased the significance of incorporating hygroscopic materials into the hydrophilic gel matrix with an appropriate network structure on the molecular scale for the AWE technology. Coupling an organic hygroscopic material with hydrophilic hydrogel may enhance composite gel desiccant system compatibility, which is well-prepared for further promotion, such as exploring a novel stimulus for gel desiccant's water desorption.

5.2 Future Direction

This thesis has developed a series of hydrogel-based porous gel desiccants composed of poly-VIM and poly-NIPAm with different structures. It displayed that the interpenetrating polymeric network structure is more suitable for moisture uptake. The future direction will firstly focus on characterization such as Scanning Electron Microscope (SEM) to disclose the resulting internal porous structure of the poly-NIPAm hydrogels. The photographs will be used to reveal the effects of synthesis temperature and composition, especially regarding the effects on hydrogels' swelling and deswelling performances. Moreover, characterization to quantify the porosity of gel desiccants will be implemented to precisely calculate surface area values and to evaluate the moisture uptake capacity of composite gel desiccants.

Apart from the characterization, feasibility research on developing novel light-responsive gel desiccant for AWE technology will be engaged. The current stimuli-responsive hydrogel-based desiccants for AWE technology are mainly designed on the photothermal or thermoresponsive. While both triggers are promising, they suffer practical problems such as energy dissipation. For example, accurate controlling the upper or lower critical solution temperature to initiate the phase transition, especially setting up the desiccant device outdoors, is a challenge for thermo-responsive mode. Therefore, it will be highly intriguing to expand stimulus possibilities, introducing a novel trigger resource from an environment-friendly, energy-saving aspect to initiate water desorption.

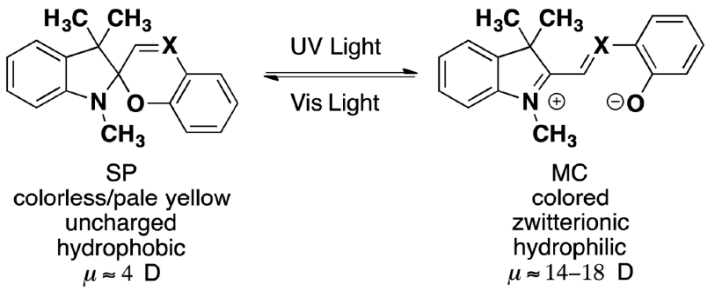

Figure 5.1. The description of isomerization of spiropyran (adapted from [95]).

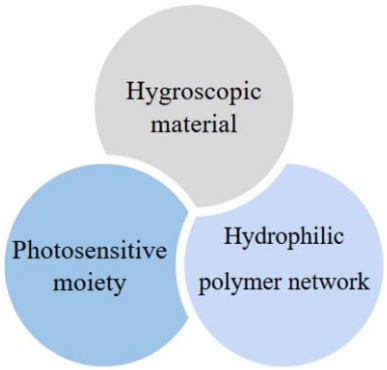

Figure 5.2. The components of light-responsive gel desiccant for AWE technology.

As discussed in chapter 2, one strategy to develop a light-responsive hydrogel incorporates the photosensitive moiety into the system. Spiropyran, a widely investigated photochromic compound, can transform reversibly from hydrophobic to hydrophilic through the photoisomerization process under particular light sources, as Figure 5.1 depicts [55,95,96]. Such a smart responsive behavior precisely caters to the next step of our work. In addition, previous works have studied poly-NIPAm-based copolymers and copolymeric hydrogels with spiropyran. For example, Ivanov and colleagues showed that the solubilities of the copolymer system could be controlled by temperature and light due to the presence of NIPAm and spiropyran [95].

For this reason, the proposed light-responsive gel desiccant system will be incorporated with spiropyran. The system takes full advantage of the function of the photosensitive moiety to initiate the volume phase transition to accomplish the purpose of liquid water recollection. Accordingly, after integrating a photosensitive moiety to the thesis's poly-VIM/poly-NIPAm IPN gel desiccant, the gel desiccant system should contain three components, as shown in Figure 5.2.

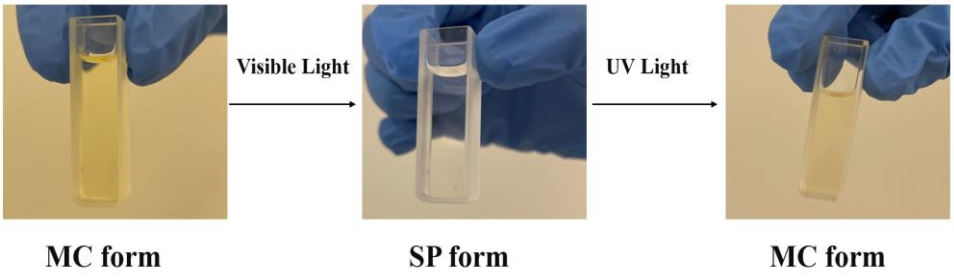

Figure 5.3. Light responsiveness test of spiropyran solution

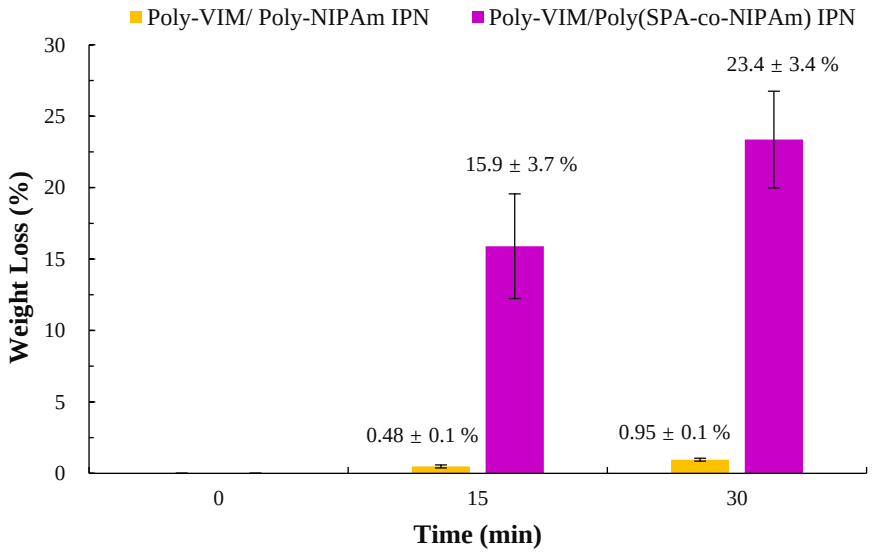

Figure 5.4. Light responsiveness tests IPN gel desiccants.

The proposed future direction is an ongoing study as Figure 5.3 directly revealed the isomerization, the form transformation of the spiropyran under the different light sources. The color change of the solution seems to agree with previous work summarized in Figure 5.1. Later, a composite gel desiccant system composed of three components with an interpenetrating polymeric network structure was developed using the low temperature synthesis method. The spiropyan was first acrylated to attach with NIPAm, and then a poly-VIM powder was embedded. Figure 5.3 showed the preliminary tests of the light-responsive behavior of such a gel desiccant. The weight loss was calculated using the following equation.

$$\text{Weight loss} = \frac{(W_{eq} - W_t)}{(W_{eq})} \text{ x } 100\%$$

Where W_{eq} is the weight of equilibrated sample at room temperature, W_t is the weight of samples at given time after exposing to the visible light.

The column chart proved that the spiropyran-contained system gradually repelled the water from its matrix upon visible light. There was hardly any water released after exposure to the light source for the control IPN gel desiccant system without spiropyran. More detailed characterization, such as moisture uptake test and cycle performance evaluation, will be implemented across a wide range of RHs. Moreover, the effect of chemical composition on composite gel desiccant system will be investigated as well. For example, the effect of the molar ratio among each monomer, and the amount of poly-VIM powder applied into the system, will be necessary for complete comprehension to explore if novel stimuli-responsive gel desiccant will fit the AWE technology in the future.

REFERENCES

[1] United Nations. 2021. Water. Available at: <http://www.un.org/en/sections/issues-depth/water/.> [Accessed from 15 Feburary 2021].

[2] Who.int. 2021. *Drinking-water*. [online] Available at: <https://www.who.int/news-room/fact-sheets/detail/drinking-water> [Accessed 15 February 2021].

[3] Wahlgren, R. V. Atmospheric water vapour processor designs for potable water production: A review. *Water Research*. **35** 1–22 (2001).

[4] Beysens, D. *et al*. Using radiative cooling to condense atmospheric vapor: A study to improve water yield. *J. Hydrol.* **276**, 1–11 (2003).

[5] Schneider, S. H. *et al*. Encyclopedia of Climate and Weather, 2nd ed.; Oxford University Press: New York, (2011).

[6] Kim, H. *et al.* Water harvesting from air with metal-organic frameworks powered by natural sunlight. *Science (80-.).* **356**, 430–434 (2017).

[7] Liu, X. *et al*. Hydrogel Machines. *Materials Today*. **36** 102–124 (2020).

[8] Larrain, H. *et al.* Fog measurements at the site 'Falda Verde' north of Chañaral compared with other fog stations of Chile. *Atmos. Res.* **64**, 273–284 (2002).

[9] Estrela, M. J. *et al*. Fog collection in the western Mediterranean basin (Valencia region, Spain). *Atmos. Res.* **87**, 324–337 (2008).

[10] Olivier, J. & De Rautenbach, C. J. The implementation of fog water collection systems in South Africa. *Atmos. Res.* **64**, 227–238 (2002).

[11] Khalil, B. *et al.* A review: dew water collection from radiative passive collectors to recent developments of active collectors. *Sustain. Water Resour. Manag.* **2**, 71–86 (2016).

[12] Mauer, L. J. & Taylor, L. S. Water-solids interactions: Deliquescence. *Annu. Rev. Food Sci. Technol.* **1**, 41–63 (2010).

[13] Kim, H. *et al.* Adsorption-based atmospheric water harvesting device for arid climates. *Nat. Commun.* **9**, 1–8 (2018).

[14] Matsumoto, K. *et al*. Thermo-responsive gels that absorb moisture and ooze water. *Nat. Commun.* **9**, 1–7 (2018).

[15] Zhao, F. *et al.* Super Moisture-Absorbent Gels for All-Weather Atmospheric Water Harvesting. *Adv. Mater.* **31**, 1806446 (2019).

[16] Bahram, M. *et al*. An Introduction to Hydrogels and Some Recent Applications. in *Emerging Concepts in Analysis and Applications of Hydrogels* (InTech, 2016). doi:10.5772/64301.

[17] Aswathy, S. *et al.* Commercial hydrogels for biomedical applications. *Heliyon*. **6** e03719 (2020).

[18] Fang, K. *et al.* Mechano-Responsive, Tough, and Antibacterial Zwitterionic Hydrogels with Controllable Drug Release for Wound Healing Applications. *ACS Appl. Mater. Interfaces* **12**, 52307–52318 (2020).

[19] Hu, J. *et al.* A pH-responsive hydrogel with potent antibacterial activity against both aerobic and anaerobic pathogens. *Biomater. Sci.* **7**, 581–584 (2019).

[20] Yin, R. *et al*. Glucose-responsive insulin delivery microhydrogels from methacrylated dextran/concanavalin A: Preparation and in vitro release study. *Carbohydr. Polym.* **89**, 117–123 (2012).

[21] Siirilä, J. *et al*. Soft poly(N-vinylcaprolactam) nanogels surface-decorated with AuNPs. Response to temperature, light, and RF-field. *Eur. Polym. J.* **115**, 59–69 (2019).

[22] Whittaker, J. *et al*. Engineering DN hydrogels from regenerated silk fibroin and poly(: N -vinylcaprolactam). *J. Mater. Chem. B* **4**, 5519–5533 (2016).

[23] Zheng, W. *et al*. Tough Al-alginate/Poly(N -isopropylacrylamide) hydrogel with tunable LCST for soft robotics. *ACS Appl. Mater. Interfaces* **7**, 1758–1764 (2015).

[24] Suzuki, A. & Tanaka, T. Phase transition in polymer gels induced by visible light. *Nature* **346**, 345–347 (1990).

[25] Salzano de Luna, M. *et al.* Light-responsive and self-healing behavior of azobenzene-based supramolecular hydrogels. *J. Colloid Interface Sci.* **568**, 16–24 (2020).

[26] Suzuki, A., Ishii, T. & Maruyama, Y. Optical switching in polymer gels. *J. Appl. Phys.* **80**, 131–136 (1996).

[27] Yeon Kim, S. *et al*. Properties of Electroresponsive Poly(vinyl alcohol)/Poly(acrylic acid) IPN Hydrogels Under an Electric Stimulus. *J Appl Polym Sci* . **73**,1675-1683 (1999).

[28] Liu, K. *et al.* A facile preparation strategy for conductive and magnetic agarose hydrogels with reversible restorability composed of nanofibrillated cellulose, polypyrrole, and Fe3O4. *Cellulose* **25**, 4565–4575 (2018).

[29] Hua, L. *et al.* Multiple-Responsive and Amphibious Hydrogel Actuator Based on Asymmetric UCST-Type Volume Phase Transition. *ACS Appl. Mater. Interfaces* **11**, 43641–43648 (2019).

[30] Cai, Y. *et al.* An enzyme-free capacitive glucose sensor based on dual-network glucose-responsive hydrogel and coplanar electrode. *Analyst* **146**, 213–221 (2021).

[31] Ren, K. *et al.* Self-healing conductive hydrogels based on alginate, gelatin and polypyrrole serve as a repairable circuit and a mechanical sensor. *J. Mater. Chem. B* **7**, 5704–5712 (2019).

[32] Dadsetan, M. *et al.* A stimuli-responsive hydrogel for doxorubicin delivery. *Biomaterials* **31**, 8051–8062 (2010).

[33] Lin, D., Lei, L., Shi, S. & Li, X. Stimulus-Responsive Hydrogel for Ophthalmic Drug Delivery. *Macromolecular Bioscience* **19,**1900001 (2019).

[34] Yu, Y. *et al.* Nanostructured lipid carrier-based pH and temperature dual-responsive hydrogel composed of carboxymethyl chitosan and poloxamer for drug delivery. *Int. J. Biol. Macromol.* **114**, 462–469 (2018).

[35] Wang, Y., Guo, J., Sun, L., Chen, H. & Zhao, Y. Dual-responsive graphene hybrid structural color hydrogels as visually electrical skins. *Chem. Eng. J.* **415**, 128978 (2021).

[36] Ouyang, J. *et al.* In situ sprayed NIR-responsive, analgesic black phosphorus-based gel for diabetic ulcer treatment. *Proc. Natl. Acad. Sci. U. S. A.* **117**, 28667–28677 (2020).

[37] Zhang, S. *et al.* A pH-responsive supramolecular polymer gel as an enteric elastomer for use in gastric devices. *Nat. Mater.* **14**, 1065–1071 (2015).

[38] Ding, M. *et al.* Multifunctional soft machines based on stimuli-responsive hydrogels: from freestanding hydrogels to smart integrated systems. *Materials Today Advances* **8**,100088 (2020).

[39] Sydney Gladman, A., Matsumoto, E. A., Nuzzo, R. G., Mahadevan, L. & Lewis, J. A. Biomimetic 4D printing. *Nat. Mater.* **15**, 413–418 (2016).

[40] Han, D. *et al.* Soft Robotic Manipulation and Locomotion with a 3D Printed Electroactive Hydrogel. *ACS Appl. Mater. Interfaces* **10**, 17512–17518 (2018).

[41] Zhang, Y. Z. *et al.* MXenes stretch hydrogel sensor performance to new limits. *Sci. Adv.* **4**, (2018).

[42] Qin, M. *et al.* Bioinspired Hydrogel Interferometer for Adaptive Coloration and Chemical Sensing. *Adv. Mater.* **30**, (2018).

[43] Altomare, L. *et al.* Biopolymer-based strategies in the design of smart medical devices and artificial organs. *International Journal of Artificial Organs* vol. 41 (2018).

[44] Katono, H. *et al.* Thermo-responsive swelling and drug release switching of interpenetrating polymer networks composed of poly(acrylamide-co-butyl methacrylate) and poly (acrylic acid). *J. Control. Release* **16**, (1991).

[45] Cooperstein, M. A. & Canavan, H. E. Assessment of cytotoxicity of (N-isopropyl acrylamide) and Poly(N-isopropyl acrylamide)-coated surfaces ARTICLES YOU MAY BE INTERESTED IN. *Biointerphases* **8**, 19 (2013).

[46] Sudhakar, K., Madhusudana Rao, K., Subha, M. C. S., Chowdoji Rao, K. & Sadiku, E. R. Temperature-responsive poly(N -vinylcaprolactam-co-hydroxyethyl methacrylate) nanogels for controlled release studies of curcumin. *Des. Monomers Polym.* **18**, (2015).

[47] Kurien, B. T. & Scofield, R. H. Increasing aqueous solubility of curcumin for improving bioavailability. *Trends in Pharmacological Sciences*. **30** (2009).

[48] Wang, Y., Zhang, L. & Wang, P. Self-Floating Carbon Nanotube Membrane on Macroporous Silica Substrate for Highly Efficient Solar-Driven Interfacial Water Evaporation. *ACS Sustain. Chem. Eng.* **4**, (2016).

[49] Chang, J. *et al.* Solar-assisted fast cleanup of heavy oil spills using a photothermal sponge. *J. Mater. Chem. A* **6**, (2018).

[50] Li, M. & Bae, J. Tunable swelling and deswelling of temperature-and light-responsive graphene oxide-poly(*N*-isopropylacrylamide) composite hydrogels. *Polym. Chem.* **11**, (2020).

[51] Wang, X., Wang, C., Zhang, Q. & Cheng, Y. Near infrared light-responsive and injectable supramolecular hydrogels for on-demand drug delivery. *Chem. Commun* **52**, 29 (2016).

[52] Li, L. *et al.* Design and Applications of Photoresponsive Hydrogels. *Adv. Mater* **31**, 1807333 (2019).

[53] Takashima, Yoshinori. et al Expansion–contraction of photoresponsive artificial muscle regulated by host–guest interactions. *Nat. Commun* **3**, 1270 (2012).

[54] Vales, T. P., Badon, I. W. T. & Kim, H. J. Multi-Responsive Hydrogels Functionalized with a Photochromic Spiropyran-Conjugated Chitosan Network. *Macromol. Res.* **26**, 950–953 (2018).

[55] Klajn, R. Spiropyran-based dynamic materials. *Chemical Society Reviews* **43**, **148-184** (2014).

[56] Zhao, C., Lu, J. & Zhu, X. X. Temperature-, Light-, and Host-Molecule-Responsive Polymers with UCST Behavior for Aqueous Sensing Applications. *ACS Appl. Polym. Mater.* **2**, 256–262 (2020).

[57] Ziółkowski, B., Florea, L., Theobald, J., Benito-Lopez Ab, F. & Diamond, D. Self-protonating spiropyran-co-NIPAM-co-acrylic acid hydrogel photoactuators. *Soft Matter*, **9,** 8754 (2013)

[58] Francis, W., Dunne, A., Delaney, C., Florea, L. & Diamond, D. Spiropyran based hydrogels actuators-Walking in the light. *Sensors Actuators B* **250**, 608–616 (2017).

[59] Li, C. *et al.* Synergistic photoactuation of bilayered spiropyran hydrogels for predictable origami-like shape change. *Matter* **4**, 1377–1390 (2021).

[60] Li, R., Shi, Y., Shi, L., Alsaedi, M. & Wang, P. Harvesting Water from Air: Using Anhydrous Salt with Sunlight. *Environ. Sci. Technol.* **52**, 5398–5406 (2018).

[61] Rô Me Canivet, J., Fateeva, A., Guo, Y., Coasne, B. & Farrusseng, D. Water adsorption in MOFs: fundamentals and applications. *This J. is Cite this Chem. Soc. Rev* **5594**, 5594 (2014).

[62] Hanikel, N., Prévot, M. S. & Yaghi, O. M. MOF water harvesters. *Nature Nanotechnology* vol. 15 (2020).

[63] Furukawa, H. *et al.* Water adsorption in porous metal-organic frameworks and related materials. *J. Am. Chem. Soc.* **136**, (2014).

[64] Li, R. *et al.* Hybrid Hydrogel with High Water Vapor Harvesting Capacity for Deployable Solar-Driven Atmospheric Water Generator. *Environ. Sci. Technol.* **52**, (2018).

[65] Ni, F. *et al.* Tillandsia-Inspired Hygroscopic Photothermal Organogels for Efficient Atmospheric Water Harvesting. *Angew. Chemie - Int. Ed.* **59**, (2020).

[66] Xu, J. *et al.* Efficient Solar-Driven Water Harvesting from Arid Air with Metal–Organic Frameworks Modified by Hygroscopic Salt. *Angew. Chemie - Int. Ed.* **59**, (2020).

[67] Ganji, F., Vasheghani-Farahani, S. & Vasheghani-Farahani, E. Theoretical description of hydrogel swelling: A review. *Iran. Polym. J. (English Ed.* **19**, (2010).

[68] Yokoyama, F., Masada, I., Shimamura, K., Ikawa, T. & Monobe, K. Morphology and structure of highly elastic poly(vinyl alcohol) hydrogel prepared by repeated freezing-and-melting. *Colloid Polym. Sci.* **264**, (1986).

[69] Chavda, H. V, Patel, C. Effect of crosslinker concentration on characteristics of superporous hydrogel. *Int. J. Pharm. Investig.* **1**, 17-21 (2011).

[70] Asayama, S., Hakamatani, T. & Kawakami, H. Synthesis and Characterization of Alkylated Poly(1-vinylimidazole) to Control the Stability of its DNA Polyion Complexes for Gene Delivery. doi:10.1021/bc900411m.

[71] Schubert, M. & Glomb, M. A. Analysis and Chemistry of Migrants from Wine Fining Polymers. *J. Agric. Food Chem* **58**, 8300–8304 (2010).

[72] Synthesis, characterization and antimicrobial activity applications of grafted copolymer alginate-g-poly(N-vinyl imidazole) | Enhanced Reader.

[73] Fares, M. M., Abu Al-Rub, F. A. & Talafha, T. Diblock Sodium Alginate Grafted Poly (N-vinylimidazole) in blank copolymeric beads and immobilized algal beads for water treatment. *Chem. Eng. Res. Des.* **153**, 603–612 (2020).

[74] Krishnan, K., Karuthapandi, S. & Vijayaraghavan, S. Ionic transport kinetics and enhanced energy storage in the electrode/poly(N-vinyl imidazole) interface for micro-supercapacitors. **10**, 45019–45027 (2020).

[75] Ahmed, E. M. Hydrogel: Preparation, characterization, and applications: A review. *Journal of Advanced Research* vol. 6 (2015).

[76] Sperling, L. H. Interpenetrating Polymer Networks: An Overview. in (1994). doi:10.1021/ba-1994-0239.ch001.

[77] Myung, D. *et al.* Progress in the development of interpenetrating polymer network hydrogels. *Polym. Adv. Technol.* **19**, (2008).

[78] Rwei, S.-P. et al. Synthesis and Characterization of pH and Thermo Dual-Responsive Hydrogels with a Semi-IPN Structure Based on N Isopropylacrylamide and Itaconamic Acid. *Materials* **11**, 696 (2018)

[79] Hu, F., Wang, Z., Zhu, B., Zhu, L. & Xu, Y. Poly (N-vinyl imidazole) gel-filled membrane adsorbers for highly efficient removal of dyes from water. *J. Chromatogr. A* **1563**, (2018).

[80] Moosavi, S. et al. Evaluation of Crosslinking Effect on Thermo-mechanical, Acoustic Insulation and Water Absorption Performance of Biomass-Derived Cellulose Cryogels. *J. Polym. Environ.* **28**, (2020).

[81] Mitchell, H., Schultz, S., Costanzo, P. & Martinez, A. Poly(N-isopropylacrylamide) Hydrogels for Storage and Delivery of Reagents to Paper-Based Analytical Devices. *Chromatography* **2**, (2015).

[82] Chatterjee, P. et al. Thermal and mechanical properties of poly(N-isopropylacrylamide)-based hydrogels as a function of porosity and medium change. *J. Appl. Polym. Sci.* **132**, 42776 (2015).

[83] Srivastava, A. *et al*. The physical characterization of supermacroporous poly(N-isopropylacrylamide) cryogel: Mechanical strength and swelling/de-swelling kinetics. *Mater. Sci. Eng. A* **464**, 93–100 (2007).

[84] Zhang, X.-Z. & Chu, C.-C. Synthesis of temperature sensitive PNIPAAm cryogels in organic solvent with improved properties. *J. Mater. Chem.* **13**, 2457–2464 (2003).

[85] Şölener, M. *et al.* A novel thermoresponsive hydrogel matrix based on poly(N- ethoxypropylacrylamide). *Polym. Bull.* **57**, 341–349 (2006).

[86] Plieva, F. M. *et al.* Pore structure in supermacroporous polyacrylamide based cryogels. *Soft Matter* **1**, 303–309 (2005).

[87] Dinu, M. *et al*. Freezing as a path to build macroporous structures: Superfast responsive polyacrylamide hydrogels. *Polymer (Guildf).* **48**, 195–204 (2007).

[88] Loo, S. L. *et al*. Design and synthesis of ice-templated PSA cryogels for water purification: Towards tailored morphology and properties. *Soft Matter* **9**, 224–234 (2013).

[89] Antonietti, M. *et al*. Morphology Variation of Porous Polymer Gels by Polymerization in Lyotropic Surfactant Phases. *Macromolecules* **32**, 1383-1389 (1999).

[90] Das.N. Preparation methods and properties of hydrogel: A review. *Int J Pharm Pharm Sci* **5**, 112-117 (2013).

[91] Aparicio-Collado, J. L. *et al.* Novel semi-interpenetrated polymer networks of poly(3-hydroxybutyrate-co-3-hydroxyvalerate)/poly (vinyl alcohol) with incorporated conductive polypyrrole nanoparticles. *Polymers (Basel).* **13**, 1–21 (2021).

[92] G O Omez Ribelles, et al. Glass transition in homogeneous and heterogeneous interpenetrating polymer networks and its relation to concentration fluctuations. *Journal of Non-Crystalline Solids*. **307–310,** 731–737 (2002).

[93] Babkina, N. V. *et al.* Effect of spatial constraints on phase separation during polymerization in sequential semi-interpenetrating polymer networks. *Polym. Sci. - Ser. A* **50**, 798–807 (2008).

[94] Mulchandani, A., Malinda, S., Edberg, J. & Westerhoff, P. Sunlight-driven atmospheric water capture capacity is enhanced by nano-enabled photothermal desiccants. *Environmental Science: Nano* **7,** 2584–2594 (2020).

[95] Balmond, E. I. *et al.* Comparative Evaluation of Substituent Effect on the Photochromic Properties of Spiropyrans and Spirooxazines. *J. Org. Chem.* **81**, 8744–8758 (2016).

[96] Ivanov, A. E., Eremeev, N. L., Wahlund, P. O., Galaev, I. Y. & Mattiasson, B. Photosensitive copolymer of N-isopropylacrylamide and methacryloyl derivative of spyrobenzopyran. *Polymer (Guildf).* **43**, 3819–3823 (2002).